A Fundamental Equation for Water Covering the Range from the Melting Line to 1273 K at Pressures up to 25 000 MPa[a)]

A. Saul and W. Wagner[b)]

Institut für Thermo- und Fluiddynamik, Ruhr-Universität Bochum, D-4630 Bochum, Federal Republic of Germany

Received May 10, 1988; revised manuscript received March 17, 1989

In order to represent the thermodynamic properties of water (H_2O) over an extremely large range of temperature and pressure that is not covered by existing equations of state, a new fundamental equation has been developed. The Helmholtz function was fitted to the following kinds of experimental data: (a) $p\rho T$ data, (b) thermal properties of the saturation curve (p_s,ρ',ρ''), (c) speed of sound w, (d) isobaric heat capacity c_p, (e) isochoric heat capacity c_v, (f) differences of the internal energy u, (g) differences of the enthalpy h, (h) Joule–Thomson coefficient μ, and (i) the isothermal throttling coefficient δ_T. A new statistical selection method was used to determine the final form of the equation from a "bank" of 630 terms which also contained functional forms that have not been previously used. This 58-coefficient equation covers the entire fluid region from the melting line to 1273 K at pressures up to 25 000 MPa, and represents the data within their experimental accuracy also in the "difficult" regions below 0 °C, on the entire saturation curve, in the critical region and at very high pressures. The equation was constrained at the critical point as defined by the parameters internationally recommended by the International Association for the Properties of Steam (IAPS). Besides the 58-coefficient equation for the entire pressure range, a 38-coefficient equation is presented for providing a "fast" equation for practical and scientific calculations in the pressure range below 1000 MPa. This equation has, with the exception of the critical region, nearly the same accuracy as the 58-coefficient equation. The quality of the new equations will be illustrated by comparing the values calculated from them with selected experimental data and with the IAPS-84 formulation and the Scaling-Law equation.

Key words: equation of state; water; thermodynamic properties.

Contents

[a)] Dedicated to Prof. Dr. phil. F. Kohler on the occasion of his 65th birthday.

[b)] To whom correspondence should be addressed.

List of Tables

List of Figures

Nomenclature

a,b,c,d	Adjustable coefficients
B	Second virial coefficient
c_p	Specific isobaric heat capacity
c_v	Specific isochoric heat capacity
c_σ	Specific heat capacity along the saturation line
C	Third virial coefficient
d	Exponent, differential
f	Specific Helmholtz energy
g	Specific Gibbs energy
h	Specific enthalpy
i,j	Indices, exponents
I,J	Upper limits of the corresponding indices
m	Index for data
M	Number of data, molar mass
p	Pressure
R	Gas constant
s	Specific entropy
t	Exponent
T	Thermodynamic temperature (no distinction is made between the thermodynamic temperature and the temperature scale defined by IPTS-68)
u	Specific internal energy
v	Specific volume
w	Speed of sound
x,y,z	General variables
α	Specific caloric property
β_s	Isentropic temperature-pressure coefficient
γ	Ratio of heat capacities ($\gamma = c_p/c_v$),
δ	Reduced density ($\delta = \rho/\rho_c$)
δ_T	Isothermal throttling coefficient
∂	Partial differential
Δ	Difference in a quantity
ϵ	Difference in the heat capacities ($\epsilon = c_p - c_v$)
Φ	Dimensionless Helmholtz energy [$\Phi = f/(RT)$]
μ	Joule-Thomson coefficient
ρ	Density
σ^2	Variance
τ	Inverse reduced temperature ($\tau = T_c/T$)
χ^2	Weighted least-squares sum according to the maximum-likelihood method

Superscripts

gen	General; full bank of terms
opt	Optimized
p	Precalculated
r	Real
$^\circ$	Ideal gas state
$''$	Saturated vapor state
$'$	Saturated liquid state
$\bar{}$	An overbar denotes a vector

Subscripts

b	At the normal boiling point ($p_b = 0.101\,325$ MPa)
c	At the critical point
calc	Calculated
exp	Experimental
0	Reference state
t	Triple point
s	Saturation

Physical constants for water (H_2O)

Molar mass	$M = 18.015\,34$ g/mol	
Gas constant	$R = 0.461\,518\,05$ J/(g K)	
Critical temperature	$T_c = 647.14$ K	cf. Ref. 16
Critical density	$\rho_c = 322$ kg/m^3	cf. Ref. 16
Critical pressure	$p_c = 22.064$ MPa	cf. Ref. 16
Reference internal energy	$u_0 = 0$	in the liquid state at the triple point
Reference entropy	$s_0 = 0$	in the liquid state at the triple point

1. Introduction

Knowledge about the thermodynamic properties of water substance is of essential importance for technical as well as for scientific applications. The increasing need for an improvement of our knowledge of the thermodynamic properties of water substance led to the international coordination of steam research early in this century. This steam research is coordinated by IAPS (International Association for the Properties of Steam). IAPS consists of scientists from several countries and it gives recommendations on the most reliable property values of water substance and on calculations involving these data in the form of Releases.

The last IAPS Release concerning equations of state for water substance was the IAPS Formulation 1984,[1] referred to as IAPS-84 in the following sections. This equation was already presented by Haar, Gallagher, and Kell[2] in 1979. It contains 48 coefficients and has a rather complicated structure that slows down computer execution time. IAPS approves a range of validity for temperatures from 273 to 1273 K at pressures up to 1000 MPa. Since IAPS-84 has some difficulties in describing the thermodynamic surface very close to the critical point, especially when considering the saturated liquid density, this region was excluded by IAPS.

Since IAPS-84 shows some further deficiencies in representing the thermodynamic surface of water (e.g., at tem-

peratures below 273 K or at pressures above 300 MPa over the whole temperature range; also, a strange behavior is observed when the equation is extrapolated to pressures above 1000 MPa), we started in 1983 to develop a new equation of state for water. At about the same time, Hill also started a research project on a new equation for water substance. In January 1987 he presented a provisional version of his equation.[3] Hill showed that he had been successful in switching from a classical analytical equation of state to the singular behavior of an extended Scaling-Law (Levelt Sengers *et al.*[4]) without producing oscillations in the derivatives in the crossover region. This equation of state is a significant step towards a representation of all experimental data within its estimated uncertainty, but the large number of 81 coefficients and the Scaling-Law part results in a rather cumbersome form which slows down computer calculations. Because of the provisional character of Hill's equation, only the Scaling-Law part[4] is used for comparisons in the enlarged critical region.

In order to avoid the problems of the existing equations of state, the following goals were formulated for the development of a new equation of state:

(a) Simultaneous fit of the new equation of state to all kinds of measured thermodynamic data in order to represent all properties within the experimental accuracy.

(b) The new equation of state should cover the whole fluid region where data exist, that is a pressure range up to 25 000 MPa (or melting pressure) at temperatures between 252 and 1273 K.

(c) Being of a simple functional form, the equation of state should be easy to handle.

(d) In order to minimize the number of coefficients, the structure of the new equation of state should be developed using an optimization method.

The steps towards the realization of these goals will be described in the following sections. A more detailed description of the work is given by Saul.[5] He gives a summary of the different sets of experimental data to which the new equation was fitted. Saul also includes statements on the uncertainty of the experimental data; cf. also Sec. 5.

2. The Helmholtz Function

The Helmholtz function is a fundamental equation with the two independent variables density ρ and temperature T. It is convenient to separate the Helmholtz function f into two parts; the ideal gas contribution $f^\circ(\rho,T)$ and the part due to the real behavior of the fluid $f^r(\rho,T)$ as follows:

$$f(\rho,T) = f^\circ(\rho,T) + f^r(\rho,T). \tag{2.1}$$

The ideal gas part $f^\circ(\rho,T)$ is obtained from an integration of a formula for the isochoric heat capacity of the ideal gas c_v°. We have used the function of Cooper.[6] It is helpful to introduce the dimensionless quantities $\tau = T_c/T$ and $\delta = \rho/\rho_c$ (the index c denotes the corresponding value at the critical point) and to normalize the Helmholtz function with the product of the gas constant R and temperature T so that:

$$\frac{f(\delta,\tau)}{RT} = \frac{f^\circ(\delta,\tau)}{RT} + \frac{f^r(\delta,\tau)}{RT}, \tag{2.2}$$

or the equivalent

$$\Phi(\delta,\tau) = \Phi^\circ(\delta,\tau) + \Phi^r(\delta,\tau). \tag{2.3}$$

The relations of the Helmholtz function to other thermodynamic properties are given in Appendix A1.

3. Fitting and Optimizing the Correlation Equation for the Helmholtz Function

The goal of this work is to present a correlation equation for the real part of the Helmholtz function $\Phi^r(\delta,\tau,\bar{a})$, where $\bar{a}$ represents the vector of coefficients to be fitted. This correlation equation must be a function linear in the coefficients a_i if the methods we used to fit the coefficients and to optimize the structure of the equation are to be applied; the reasons for this statement will be given later in this section. For the structure of the equation of state, we will consider characteristics such as the functional type (pure polynomials, polynomials coupled with exponential functions with regard to density etc.), the exponents of the density and temperature terms in the equation, ways of combining different functional types, and last but not least the number of coefficients.

Some examples of the thermodynamic relations of the Helmholtz function to the various properties $z_j(\Phi,\delta,\tau,\bar{a})$ are given in Table 1, namely the pressure p, the enthalpy h, the isobaric heat capacity c_p, and difference of the internal energy u.

Besides some theoretical assumptions which must be considered when developing an equation of state, experimental data $z_{\text{exp}}(x_{\text{exp}},y_{\text{exp}})$ are the only information available about the thermodynamic surface, where x,y, and z denote general thermodynamic variables. One tries to fit Φ^r to the experimental data in such a way that the weighted sum of squares:

$$\chi_j^2 = \sum_{m=1}^{M_j} \left(\frac{[z_{\text{exp}} - z(\Phi,x_{\text{exp}},y_{\text{exp}},\bar{a}]^2}{\sigma_{\text{exp}}^2} \right)_{j,m} = \sum_{m=1}^{M_j} \frac{\Delta z_{j,m}^2}{\sigma_{j,m}^2}, \tag{3.1}$$

is minimized. In Eq. (3.1) σ^2 corresponds to the total uncertainty of the experimental data according to the Gaussian error propagation formula. The index j in Eq. (3.1) denotes one particular property j that is being considered. When an equation of state is fitted to more than one property, it is called a simultaneous or multiproperty fit and the resulting sum of squares:

$$\chi^2 = \sum_{j=1}^{J} \chi_j^2, \tag{3.2}$$

is to be minimized. The problem of minimizing the sum of squares becomes a problem of solving simultaneously a system of normal equations. Depending on the property to which the equation is fitted, the system of equations becomes linear or nonlinear. If the relation between the property z_j and the Helmholtz function is a linear combination of Φ and its derivatives, then the basic requirement for a system of linear equations for the coefficient vector $\bar{a}$ is satisfied. Such linear relations in Φ and its derivatives are those for the pressure p, the enthalpy h, and for the difference of the internal energy u as listed in Table 1. Unfortunately, most experimentalists actually measure the thermodynamic properties

TABLE 1. Examples of relations of thermodynamic properties to the Helmholtz function and its derivatives.

Property	Relation	Precorrelation of
Pressure $z_j = p(\rho,T)$	explicit	
$\frac{p(\delta,\tau)}{\rho RT} = 1 + \delta\Phi^r_\delta$ [a]	linear	
Enthalpy $z_j = h(p,T)$	implicit	ρ^p
$\frac{h(\delta,\tau)}{RT_c} = \tau^{-1}(1+\delta\Phi^r_\delta) + \Phi^0_\tau + \Phi^r_\tau$	linear	
Isobaric heat capacity $z_j = c_p(p,T)$	implicit	ρ^p
$\frac{c_p(\delta,\tau)}{R} = -\tau^2(\Phi^0_{\tau\tau} + \Phi^r_{\tau\tau}) + \underbrace{\frac{(1+\delta\Phi^r_\delta - \delta\tau\Phi^r_{\delta\tau})^2}{1+2\delta\Phi^r_\delta + \delta^2\Phi^r_{\delta\delta}}}_{\epsilon^p}$	non-linear	ϵ^p
Difference of the internal energy $z_j = u(\rho,T)$	explicit	
$\frac{u_2}{RT_c} - \frac{u_1}{RT_c} = \Phi^0_\tau(\tau_2) + \Phi^r_\tau(\delta_2,\tau_2) - \Phi^0_\tau(\tau_1) - \Phi^r_\tau(\delta_1,\tau_1)$	linear	

[a] Φ_δ denotes the partial derivative $\left(\frac{\partial\Phi}{\partial\delta}\right)_\tau$, similarly: $\Phi_\tau = \left(\frac{\partial\Phi}{\partial\tau}\right)_\delta$, $\Phi_{\delta\delta} = \frac{\partial^2\Phi}{\partial\delta^2}$, $\Phi_{\tau\tau} = \frac{\partial^2\Phi}{\partial\tau^2}$, $\Phi_{\delta\tau} = \frac{\partial^2\Phi}{\partial\delta\partial\tau}$.

as a function of pressure p and temperature T (e.g., the enthalpy h) and not as a function of density ρ and temperature T, which are the independent variables of the Helmholtz function f. This yields an implicit relation between the measured state variables p and T and the independent variables ρ and T of the Helmholtz function and leads to a system of nonlinear equations for the coefficients of the equation of state.

Moreover, there exist thermodynamic properties whose relations to the Helmholtz function are not linear combinations of Φ and its derivatives; an example is the isobaric heat capacity c_p (cf. Table 1). A fit to these properties will also result in a system of nonlinear equations for $\bar{a}$. Those properties which lead to a system of linear equations when calculating the coefficient vector $\bar{a}$ will now be called "linear", and the others will be called "nonlinear" properties. Solving a system of nonlinear equations can involve extensive computer time, but this problem can be solved.

At this point we should recall that the correlation equation for the Helmholtz function must be a linear function of the coefficients a_i. This is caused by the fact that nonlinear least-squares methods malfunction if the coefficients and the exponents of the density and temperature functions are to be determined simultaneously. The determination of optimized exponents means an optimization of the structure of the function and this can, at present, only be managed if Φ is a linear combination of all the adjustable coefficients a_i. The structures of most of the existing equations of state have been determined subjectively based on the experience of the researcher or by trial and error. In order to overcome this unsatisfactory situation of trial and error, Wagner[7] developed optimization strategies which have been proven for many thermodynamic functions, i.e., vapor pressure equations. For complex structures like an equation of state, the very computer-time-intensive Evolutionary Optimization Method (EOM) of Ewers and Wagner[8] is superior to the very fast regression analysis of Wagner.[7] The optimization method used in this work was recently developed by Setzmann and Wagner,[10] and combines both the reliability of the EOM and the high speed of convergence of the regression analysis of Wagner.

All of the optimization strategies require a general comprehensive functional formulation called a "bank of terms". On the basis of a mathematical and statistical analysis, the optimization procedure selects out of this bank of terms the most effective correlation equation for the problem formulated by the data. The main disadvantage of all of these optimization methods is the fact that they can only find the best structure when the optimization problem consists of linear data. It was one of the major objectives of this work to make the nonlinear-data information available for our optimization method. In order to linearize an implicit relation, e.g., for the enthalpy $h(p,T)$ (cf. Table 1), it is sufficient to precalculate the density ρ^p for the measured pressure p and the temperature T from a known equation of state (the best one that is available). For an implicit nonlinear relation (e.g., the isobaric heat capacity c_p, cf. Table 1) one must precalculate the density ρ^p as well as a characteristic variable that linearizes the relation between the property to be fitted and Φ and its derivatives (e.g., for c_p the term ϵ^p). For some properties in selected regions (e.g., vapor–liquid equilibrium, dilute-gas region), a data synthesis, i.e., the calculation of state values from a known equation but not necessarily an equation of state, was performed. A summary of the individual sums of least squares used for the nonlinear simultaneous fit as well as for the optimization procedure is given in Table 2.

4. The Method of Simultaneous Improvement of the Equation of State and the Data Set

Figure 1 shows the steps within one cycle of the development of our equation of state. Proceeding from the equa-

TABLE 2. Contributions of the properties to the sum of least squares [Eq. (3.2)] for fitting and optimizing the new correlation equation for the Helmholtz function.

j	Data x,y,z	Sum of weighted least squares $\chi_j^2 = \sum_{m=1}^{M_j} \Delta z_{j,m}^2 \sigma_{j,m}^{-2}$ according to Eq. (3.1)	
1	p,ρ,T	$\sum_{m=1}^{M_1+M_2+M_3} \left[\frac{p-\rho RT}{\rho^2 RT} - \rho_c^{-1}\Phi_\delta^r\right]_m^2 \sigma_{j,m}^{-2}$	(3.3)
2	p_s,ρ',T		
3	p_s,ρ'',T		
4	Maxwell criterion	$\sum_{m=1}^{M_4}\left[\frac{p_s}{RT\rho''}\left(1-\frac{\delta''}{\delta'}\right) - \ln\left(\frac{\delta'}{\delta''}\right) - \Phi' + \Phi''\right]_m^2 \sigma_{4,m}^{-2}$	(3.4)
5	c_v,ρ,T	$\sum_{m=1}^{M_5}\left[\frac{c_v}{R} + \tau^2(\Phi_{\tau\tau}^0 + \Phi_{\tau\tau}^r)\right]_m^2 \sigma_{5,m}^{-2}$	(3.5)
6	u_1,ρ_1,T_1 u_2,ρ_2,T_2	$\sum_{m=1}^{M_6}\left[\frac{u_2}{RT_c} - \frac{u_1}{RT_c} - (\Phi_\tau^0 + \Phi_\tau^r)_2 + (\Phi_\tau^0 + \Phi_\tau^r)_1\right]_m^2 \sigma_{6,m}^{-2}$	(3.6)
7	h_1,ρ_1^ρ,T_1 h_2,ρ_2^ρ,T_2	$\sum_{m=1}^{M_7}\left[\frac{h_2}{RT_c} - \frac{h_1}{RT_c} - (\tau^{-1}(1+\delta\Phi_\delta^r) + \Phi_\tau^0 + \Phi_\tau^r)_2 + (\tau^{-1}(1+\delta\Phi_\delta^r) + \Phi_\tau^0 + \Phi_\tau^r)_1\right]_m^2 \sigma_{7,m}^{-2}$	(3.7)
8[a]	h_1,p_1,T_1 h_2,p_2,T_2	$\sum_{m=1}^{M_8}\left[\frac{h_2}{RT_c} - \frac{h_1}{RT_c} - (\tau^{-1}(1+\delta\Phi_\delta^r) + \Phi_\tau^0 + \Phi_\tau^r)_2 + (\tau^{-1}(1+\delta\Phi_\delta^r) + \Phi_\tau^0 + \Phi_\tau^r)_1\right]_m^2 \sigma_{8,m}^{-2}$	(3.8)
9[a]	$c_\rho,\rho^\rho,T,\varepsilon^\rho$	$\sum_{m=1}^{M_9}\left[\frac{c_\rho}{R} + \tau^2(\Phi_{\tau\tau}^0 + \Phi_{\tau\tau}^r) - \varepsilon^\rho\right]_m^2 \sigma_{9,m}^{-2}$	(3.9)
10[a]	c_p,p,T	$\sum_{m=1}^{M_{10}}\left[\frac{c_p}{R} + \tau^2(\Phi_{\tau\tau}^0 + \Phi_{\tau\tau}^r) - \frac{(1+\delta\Phi_\delta^r - \delta\tau\Phi_{\delta\tau}^r)^2}{1+2\delta\Phi_\delta^r + \delta^2\Phi_{\delta\delta}^r}\right]_m^2 \sigma_{10,m}^{-2}$	(3.10)
11	$w,\rho^\rho,T,\gamma^\rho$	$\sum_{m=1}^{M_{11}}\left[\frac{w^2}{RT} - \gamma^\rho(1+2\delta\Phi_\delta^r + \delta^2\Phi_{\delta\delta}^r)\right]_m^2 \sigma_{11,m}^{-2}$	(3.11)
12[a]	w,p,T	$\sum_{m=1}^{M_{12}}\left[\frac{w^2}{RT} - 1 - 2\delta\Phi_\delta^r - \delta^2\Phi_{\delta\delta}^r + \frac{(1+\delta\Phi_\delta^r - \delta\tau\Phi_{\delta\tau}^r)^2}{\tau^2(\Phi_{\tau\tau}^0 + \Phi_{\tau\tau}^r)}\right]_m^2 \sigma_{12,m}^{-2}$	(3.12)
13[a]	μ,p,T	$\sum_{m=1}^{M_{13}}\left[\mu R\rho + \frac{(\delta\Phi_\delta^r + \delta^2\Phi_{\delta\delta}^r + \delta\tau\Phi_{\delta\tau}^r)}{(1+\delta\Phi_\delta^r - \delta\tau\Phi_{\delta\tau}^r)^2 - \tau^2(\Phi_{\tau\tau}^0 + \Phi_{\tau\tau}^r)(1+2\delta\Phi_\delta^r + \delta^2\Phi_{\delta\delta}^r)}\right]_m^2 \sigma_{13,m}^{-2}$	(3.13)
14[a]	δ_T,p,T	$\sum_{m=1}^{M_{14}}\left[\delta_T\rho - 1 + \frac{1+\delta\Phi_\delta^r - \delta\tau\Phi_{\delta\tau}^r}{1+2\delta\Phi_\delta^r + \delta^2\Phi_{\delta\delta}^r}\right]_m^2 \sigma_{14,m}^{-2}$	(3.14)

Where $\sigma_{j,m}^2$, according to the gaussian error propagation formula, is given by:

$$\sigma_{j,m}^2 = \left[\left(\frac{\partial \Delta z}{\partial x}\right)_{y,z}^2 \sigma_x^2 + \left(\frac{\partial \Delta z}{\partial y}\right)_{x,z}^2 \sigma_y^2 + \left(\frac{\partial \Delta z}{\partial z}\right)_{x,y}^2 \sigma_z^2\right]_{j,m} \tag{3.15}$$

The functional structure has been optimized (opt) according to the following least square sum:

$$\chi_{\text{opt}}^2 = \chi_1^2 + \chi_2^2 + \chi_3^2 + \chi_4^2 + \chi_5^2 + \chi_6^2 + \chi_7^2 + \chi_9^2 + \chi_{11}^2 \tag{3.16}$$

The final coefficients were obtained from minimizing the following least square sum by a nonlinear fit (nl):

$$\chi_{nl}^2 = \chi_1^2 + \chi_2^2 + \chi_3^2 + \chi_4^2 + \chi_5^2 + \chi_6^2 + \chi_8^2 + \chi_{10}^2 + \chi_{12}^2 + \chi_{13}^2 + \chi_{14}^2 \tag{3.17}$$

[a] A fit to these properties will lead to systems of nonlinear equations where the following coupling condition has to be taken into account: $p = \rho RT(1+\delta\Phi_\delta^r)$ (3.18)

tion of state resulting from the previous cycle, an examination of both the equation of state and the data set is performed. This examination is commonly based on deviation or absolute plots, keeping in mind the often very optimistic estimates of the experimentalists with regard to the accuracy of their experimental data. A well-founded knowledge of the experimental data is required. Factors to be considered include the reliability and reputation of the experimental group, the fluid regions covered, and the comments of other, independent evaluators. This, together with considerable experience, will help us decide whether to: (a) change weighting, (b) add data, (c) reject data, (d) "thin out" in regions where data are abundant, (e) "correct" data, or (f) "synthesize" data. With the aid of the equation of state resulting from the previous cycle, a new linear data set for the optimization and a nonlinear one for the nonlinear simultaneous fitting procedure results. This means that a new synthesis, precalculation, and weighting is performed for every new cycle.

On the other hand, one should always consider whether the functional structures forming the bank of terms are actually able to describe the problem defined by the data. We performed a systematic study on this problem and will return to it in Sec. 6.

Based on the linear data set, the optimization procedure selects the most effective equation of state; a minimizing of

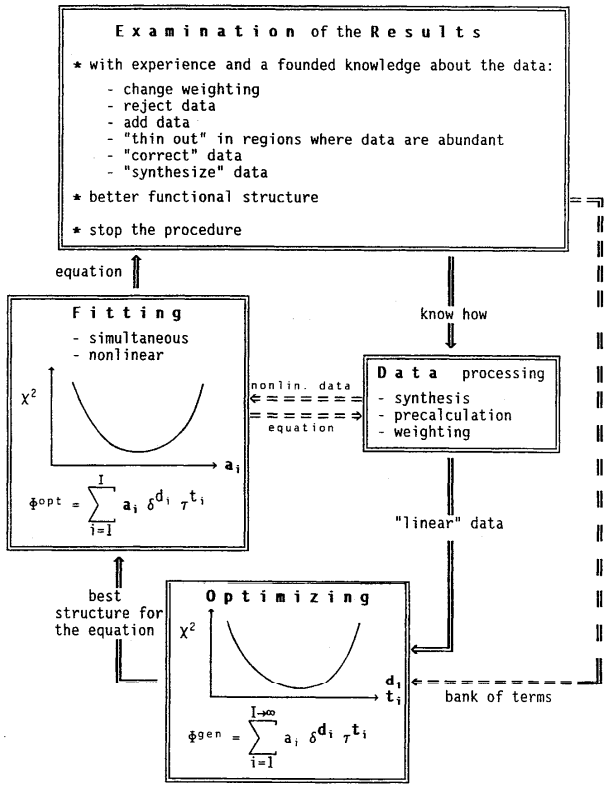

FIG. 1. The steps within one cycle during the development of the new equation of state.

the sum of squares with regard to the exponents d_i and t_i (cf. Fig. 1) takes place. Based on the nonlinear (original) data set, the subsequent nonlinear fitting procedure minimizes the sum of squares with regard to the coefficient vector $\bar{a}$ of the new equation of state; now the cycle is complete.

Every cycle of this procedure improves the equation of state as well as the linear data set. At the end of this iterative procedure the data set becomes very stable and no further improvement of the equation of state is possible; the final equation is obtained.

At this stage we would emphasize that the precalculation and data synthesis were only used to make the nonlinear-data information available for the linear optimization procedure. Comparisons were always made with respect to the original linear and nonlinear data.

5. The Data Set for Water Substance

One task of IAPS has been the review of experimental data on the thermophysical properties of steam and water substance. Based on this extensive work carried out over several decades (cf. the latest review by Sato *et al.*[9]) and on our own data evaluation including a judgment of the experimental uncertainties, we have selected the data set used to fit the new equations.

In addition to an overview of the selected data set (details can be found in Ref. 5), we will show in this section how we constrained the equation of state in regions where only nonlinear data or no data were available. The following statements should be considered when reading this section:

1. It was the goal of our work to represent the reliable data on *all properties* within the experimental uncertainty.

2. The new equation of state was constrained to yield a physically meaningful behavior in regions where data exist as well as in regions where no data are available.

3. The coefficient vector of the final equation of state was determined by a direct simultaneous nonlinear fit to the *original data*.

Consistent with point 1 we considered it acceptable to create artificial linear data, i.e., to perform a *data synthesis* in order to improve the quality of the optimized equation of state with respect to the nonlinear data.

This was done at 218 temperatures where we calculated values for the vapor pressure p_s, the saturated liquid density ρ' and the saturated vapor density ρ'' from our equations for the saturation line.[11] The values resulting from these equations, recently recommended by IAPS, were used to define the Maxwell criterion for our new equation of state. In order to yield a better representation of the caloric properties along the saturation line, we also calculated: (a) 74 differences of the internal energy of the saturated liquid $[u'(\rho',T)_2 - u'(\rho',T)_1]$ and (b) 75 internal energies of vaporization $[u''(\rho'',T) - u'(\rho',T)]$ from the equations given in Ref. 11.

As a first step towards a representation of all available data in the low-density region, we established a virial equation for the region below 55 kg/m^3 ($\simeq 0.17\,\rho_c$) at temperatures from 273 to 1123 K (cf. Saul[5]). When establishing this equation we adopted the procedure of successive improvement of the data set and the equation of state as we described in Secs. 3 and 4. The virial equation was then generally used for the precalculation and for the data synthesis within the range of its validity, i.e., after establishing this equation, the data set for this region remained unchanged.

We calculated 75 state values from this equation for the linear data set. The calculation was performed for the following properties: (a) $p\rho T$, (b) velocity of sound w, and (c) isochoric heat capacity c_v. This was found to yield a well behaved surface from the equation of state in this region. For the final nonlinear fitting of the coefficients a_i, 25 of the 75 artificial data were not used because that region was covered by experimental Joule–Thomson- and isothermal throttling-coefficient data.

The complete data set for water substance is shown schematically in Fig. 2 on the pT plane, whereas Table 3 gives an overview of the experimental and artificial data that we used for our 58-coefficient equation of state. The data set used for the development of our 38-coefficient equation of state is a subset ($273.16\ \text{K} \leqslant T \leqslant 1273\ \text{K}$; $0\ \text{MPa} < p \leqslant 400\ \text{MPa}$) of these selected data. Where needed, the units of the original data were converted into SI units. The temperatures of those measurements which did not correspond to the IPTS-68 (International Practical Temperature Scale of 1968) were converted according to IPTS-68.

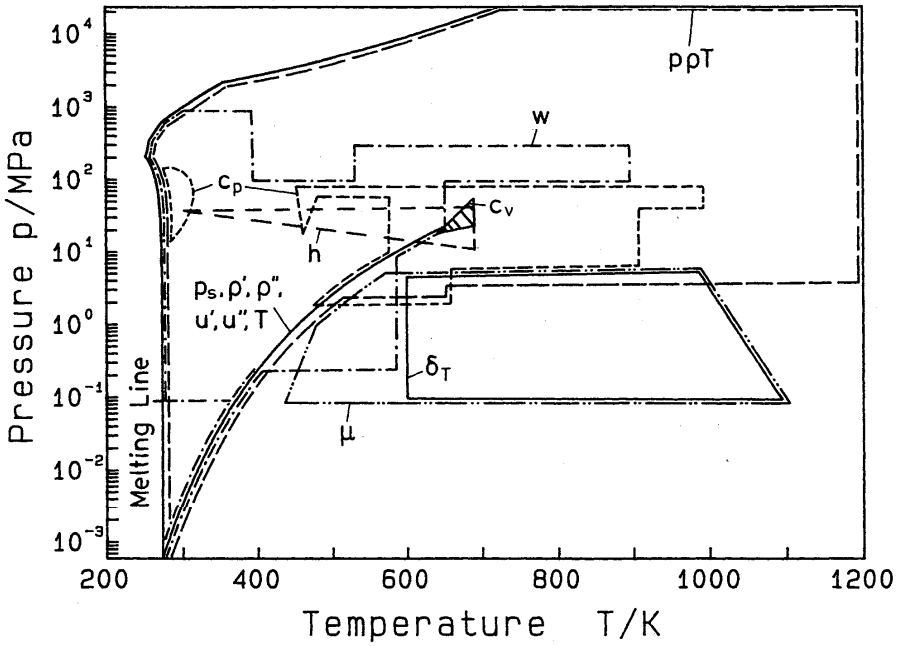

FIG. 2. The distribution of the experimental data of the different properties used for fitting the new equation of state in a pT diagram.

TABLE 3. Pooling of the data set used for the nonlinear simultaneous fit and for the optimization procedure.

Data	Remarks	Number of data when: optimizing	fitting nonlinearly
p,ρ,T	original data	2538	2538
p_s,ρ',T	calc. Ref. 11	218	218
p_s,ρ'',T	calc. Ref. 11	218	218
p,ρ,T	calc. Ref. 5	75	55 below 480 K
Maxwell-crit.	calc. Ref. 11	218	218
c_v,ρ,T	original data	116	116
c_v,ρ,T	calc. Ref. 5	75	55 below 480 K
w,p,T	original data		418
w,ρ^p,γ^p,T	precalculated data	418	
w',p_s,T	original data		47
w',ρ^p,γ^p,T	precalculated data	47	
w'',p_s,T	original data		50
$w'',\rho^p\gamma^p,T$	precalculated data	50	
w,p,T	calc. Ref. 5		55 below 480 K
w,ρ^p,γ^p,T	calc. Ref. 5	75	
c_p,p,T	original data		765
c_p,ρ^p,ϵ^p,T	precalculated data	765	
h_1,p_1,T_1 h_2,p_2,T_2	original data		235
h_1,ρ^p,T_1 h_2,ρ^p,T_2	precalculated data	235	
μ,p,T	original data		234
δ_T,p,T	original data		180
$(u',\rho',T)_1$ $(u',\rho',T)_2$	calc. Ref. 11	74	74
$u''-u',\rho'',\rho',T$	calc. Ref. 11	75	75
Sum		5197	5551

6. Examination of Functional Structures for the Correlation Equation of the Helmholtz Function

We will now give a brief summary of the results of our analysis on the functional structures considered when developing the new equation of state. Based on our experience with the development of an equation of state for oxygen,[12–14] we evaluated four families of functional structures when establishing the new equation of state, namely:

E terms: $$\sum_{j=0}^{6} e^{-\delta^j} \sum_{i=1}^{I_j} a_{1,ij} \delta^{d_{ij}} \tau^{t_{ij}} \tag{6.1}$$

(E-1) terms: $$\sum_{j=1}^{3} (e^{-\delta^j} - 1) \sum_{i=1}^{I_j} a_{2,ij} \delta^{d_{ij}} \tau^{t_{ij}} \tag{6.2}$$

(E6-E6) terms: $$(e^{-0.4\delta^6} - e^{-2\delta^6}) \sum_{i=1}^{I} a_{3,i} \delta^{d_i} \tau^{t_i} \tag{6.3}$$

Gaussian terms: $$e^{-30(\delta-1)^2 - 100(\tau-1)^2} \sum_{i=1}^{I} a_{4,i} \delta^{d_i} \tau^{t_i}. \tag{6.4}$$

The amount of computer time and the amount of memory required for optimizing an equation of state increases quadratically with the number of terms considered. This led us to restrict the number of terms to about 650. Consequently, we could not evaluate all possible structures at the same time and we had to split the entire set into a partial bank of terms.

The most effective contribution of the E terms to the final equation of state was obtained from the terms where

$j = 0,1,2,3$. In contrast to our equation of state for oxygen (cf. Ref. 13) we did not need the E terms for $j = 4$. The use of (E-1) terms as well as the use of the Gaussian terms was found to yield no essential improvement in the representation of the data. Therefore, these families of functions were not considered when establishing the final bank of terms. The (E6-E6) terms, however, were found to improve clearly the representation of the thermal as well as the caloric properties within the critical region. Thus, the final bank of terms for the real part of the Helmholtz function consisted of the follwing terms:

$$\Phi^{r,\mathrm{gen}} = \sum_{i=1}^{13}\sum_{j=0}^{13} a_{1,ij}\delta^i\tau^j + e^{-\delta^1}\sum_{i=1}^{11}\sum_{j=0}^{13} a_{2,ij}\delta^i\tau^j + e^{-\delta^2}\sum_{i=1}^{11}\sum_{j=0}^{13} a_{3,ij}\delta^i\tau^j + e^{-\delta^3}\sum_{i=1}^{5}\sum_{j=13}^{26} a_{4,ij}\delta^i\tau^j + (e^{-0.4\delta^6} - e^{-2\delta^6})\sum_{i=1}^{5}\sum_{j=12}^{25} a_{5,ij}\delta^i\tau^{2j}. \quad (6.5)$$

The bank of terms defined by Eq. (6.5) contains 630 terms and was used to establish our 58-coefficient equation of state. For the 38-coefficient equation of state the $e^{-\delta^1}$ terms (second functional form in Eq. (6.5)) and the (E6-E6) terms were not considered. This bank of terms only contained 396 terms. The range of the density and temperature exponents for each bank of terms was chosen based on the results from several runs of our optimization procedure.

7. The Correlation Equations for the Helmholtz Function

The complete Helmholtz function can be written as

$$\frac{f(\delta,\tau)}{RT} = \frac{f^\circ(\delta,\tau)}{RT} + \frac{f^r(\delta,\tau)}{RT}, \quad (7.1)$$

where $\tau = T_c/T$, $\delta = \rho/\rho_c$.

The ideal part of the Helmholtz function $f^\circ(\delta,\tau)/(RT)$ was obtained from Cooper's[6] c_p° equation and is based on the c_p° data of Woolley.[15] The Cooper equation is valid for the temperature region $130\ \mathrm{K} \leqslant T \leqslant 4000\ \mathrm{K}$ and has, expressed in Φ°, the following form:

$$\Phi^\circ = \frac{f^\circ}{RT} = \ln(\delta) + a_1^\circ + a_2^\circ\tau + a_3^\circ\ln(\tau) + \sum_{i=4}^{8} a_i^\circ\ln(1 - e^{-\gamma_i^\circ\tau}), \quad (7.2)$$

where $\tau = T_c/T$, $\delta = \rho/\rho_c$ and

i	a_i°	γ_i°	i	a_i°	γ_i°
1	cf. Sec. 7.1 or 7.2		5	0.973 150	3.537 101 709
2	cf. Sec. 7.1 or 7.2		6	1.279 500	7.740 210 774
3	3.006 320		7	0.969 560	9.243 749 421
4	0.012 436	1.287 202 151	8	0.248 730	27.505 640 200

$T_c = 647.14$ K, $\rho_c = 322$ kg/m^3, and $R = 0.461\ 518\ 05$ J/(g K)

The constants γ_i° of the original Cooper paper were revised (divided by T_c) in order to use the same dimensionless temperature for the independent variable as for the real part of the Helmholtz function. The constants a_1° and a_2° were adjusted so that Eq. (7.1) yields zero values for the entropy and the internal energy in the saturated liquid state at the triple point. This leads to different numerical values of a_1° and a_2° for the two equations given in the following subsections. In Appendix A2 we will explicitly give all required derivations of the ideal part as well as for the real part of the Helmholtz function with respect to δ and τ.

7.1. The 58-Coefficient Equation of State

The complete Helmholtz function is given by Eq. (7.1). The constants a_1° and a_2° for the ideal part of the Helmholtz function $f^\circ(\delta,\tau)/(RT)$, cf. Eq. (7.2), have the following numerical values: $a_1^\circ = -8.318\ 441$, $a_2^\circ = 6.681\ 816$.

Based on the bank of terms defined by Eq. (6.5) and the available data sources (cf. Table 3), the following real part of the Helmholtz function $\Phi^r = f^r(\delta,\tau)/(RT)$ was determined using the procedure as described in Sec. 4:

$$\Phi^r = \frac{f^r(\delta,\tau)}{RT} = \sum_{i=1}^{I_1}(a_i\delta^{d_i}\tau^{t_i}) + \sum_{i=I_1+1}^{I_2} e^{-\delta^{\gamma_i}}(a_i\delta^{d_i}\tau^{t_i}) + (e^{-0.4\delta^6} - e^{-2\delta^6})\sum_{i=55}^{58}(a_i\delta^{d_i}\tau^{t_i}), \quad (7.3)$$

where $\tau = T_c/T$, $\delta = \rho/\rho_c$, and $I_1 = 9$, $I_2 = 54$.

The final coefficients of this new equation of state were obtained by a nonlinear least-squares fit to the selected data. Table 4 gives the coefficients and parameters of this 58-coefficient equation of state, Eq. (7.3).

The equation of state was developed on the basis of data which cover the region $252\ \mathrm{K} \leqslant T \leqslant 1273\ \mathrm{K}$, $0\ \mathrm{MPa} < p \leqslant 25\,000\ \mathrm{MPa}$ (or melting pressure).

The equation of state was constrained to the internationally recommended values for the critical parameters (see the paragraph "Physical constants" in the Nomenclature). The data of all measured properties (thermal and caloric properties) are represented within their estimated uncertainty; the only exception is a single experimental c_v value closest to the critical point.

TABLE 4. Parameters and coefficients of the new 58-coefficient equation of state, Eq. (7.3).

i	γ_i	d_i	t_i	a_i
1		1	0	0.821 637 747 8
2		1	2	−0.254 389 437 9
3		2	0	$-0.883\,086\,864\,8\times10^{-1}$
4		5	9	$-0.890\,309\,724\,8\times10^{-6}$
5		8	0	$-0.124\,133\,335\,7\times10^{-5}$
6		11	0	$0.289\,559\,028\,6\times10^{-8}$
7		11	12	$0.140\,361\,030\,9\times10^{-10}$
8		13	7	$0.818\,394\,337\,1\times10^{-12}$
9		13	13	$-0.239\,790\,528\,7\times10^{-12}$
10	1	1	0	−0.751 974 334 1
11	1	1	1	−0.415 127 858 8
12	1	1	3	$-0.103\,051\,374\,0\times10^{1}$
13	1	2	1	$-0.164\,803\,688\,8\times10^{1}$
14	1	2	5	−0.468 635 025 1
15	1	3	5	0.356 025 814 2
16	1	4	2	−0.636 465 829 4
17	1	4	3	0.222 748 236 3
18	1	4	5	$-0.895\,484\,993\,9\times10^{-1}$
19	1	5	6	$0.155\,768\,678\,8\times10^{-2}$
20	1	6	4	$0.134\,771\,908\,8\times10^{-2}$
21	1	7	1	$-0.130\,135\,338\,5\times10^{-2}$
22	1	8	8	$0.998\,736\,867\,3\times10^{-6}$
23	1	9	0	$0.226\,362\,947\,6\times10^{-3}$
24	1	11	1	$0.289\,330\,495\,0\times10^{-5}$
25	2	1	0	0.199 543 716 9
26	2	1	9	$-0.270\,776\,766\,2\times10^{-1}$
27	2	1	10	$0.184\,906\,821\,6\times10^{-1}$
28	2	1	11	$-0.440\,239\,435\,7\times10^{-2}$
29	2	2	0	$-0.854\,687\,673\,7\times10^{-1}$
30	2	2	8	0.122 053 857 6
31	2	4	5	−0.256 223 704 1
32	2	5	4	0.255 503 463 6
33	2	6	2	$-0.632\,320\,390\,7\times10^{-1}$
34	2	6	12	$0.335\,139\,757\,5\times10^{-4}$
35	2	7	3	$-0.615\,283\,498\,5\times10^{-1}$
36	2	7	10	$-0.353\,304\,820\,8\times10^{-3}$
37	2	8	3	$0.314\,630\,925\,9\times10^{-1}$
38	2	10	2	$-0.226\,179\,598\,3\times10^{-2}$
39	2	10	8	$0.186\,897\,020\,0\times10^{-3}$
40	2	11	0	$-0.138\,461\,455\,6\times10^{-2}$
41	2	11	1	$0.271\,316\,007\,3\times10^{-2}$
42	2	11	3	$-0.486\,611\,853\,9\times10^{-2}$
43	2	11	4	$0.375\,178\,912\,9\times10^{-2}$
44	2	11	6	$-0.569\,266\,937\,3\times10^{-3}$
45	3	2	13	−0.587 641 455 5
46	3	2	14	0.568 783 834 6
47	3	2	15	−0.164 215 819 8
48	3	3	14	0.587 863 588 5
49	3	3	16	−0.284 430 193 1
50	3	4	13	−0.204 919 833 7
51	3	4	26	$-0.403\,923\,371\,6\times10^{-2}$
52	3	5	15	$0.545\,904\,959\,4\times10^{-1}$
53	3	5	23	$-0.891\,426\,014\,6\times10^{-2}$
54	3	5	25	$0.497\,441\,125\,4\times10^{-2}$
55		1	50	$-0.709\,318\,338\,0\times10^{-2}$
56		2	40	$0.171\,879\,634\,2\times10^{-1}$
57		3	32	$-0.148\,265\,303\,8\times10^{-1}$
58		4	26	$0.451\,729\,288\,4\times10^{-2}$

$T_c = 647.14$ K, $\rho_c = 322$ kg/m^3, $R = 0.461\,518\,05$ J/(g K)

7.2. The 38-Coefficient Equation of State

Once again, the complete Helmholtz function is given by Eq. (7.1). The constants a_1° and a_2° for the ideal part of the Helmholtz function $f^\circ(\delta,\tau)/(RT)$, cf. Eq. (7.2), have the following numerical values: $a_1^\circ = -8.317\,709\,5$, $a_2^\circ = 6.681\,504\,9$.

Based on the bank of terms given in Sec. 6 and the available data sources (cf. Sec. 5), the following real part of the Helmholtz function Φ^r was determined:

$$\Phi^r = \frac{f^r(\delta,\tau)}{RT} = \sum_{i=1}^{I_1} (a_i \delta^{d_i} \tau^{t_i}) + \sum_{i=I_1+1}^{I_2} e^{-\delta^{\gamma_i}} (a_i \delta^{d_i} \tau^{t_i}), \tag{7.4}$$

where $\tau = T_c/T$, $\delta = \rho/\rho_c$, and $I_1 = 12$, $I_2 = 38$.

The final coefficients of this equation of state were obtained by a nonlinear least-squares fit to the selected data. Table 5 gives the coefficients and parameters of this 38-coefficient equation of state, Eq. (7.4).

The equation of state was developed using data in the region 273.16 K $\leqslant T \leqslant$ 1273 K, 0 MPa $< p \leqslant$ 400 MPa.

The equation of state was constrained to the internationally recommended values for the critical parameters (T_c = 647.14 K, ρ_c = 322 kg/m^3, p_c = 22.064 MPa, cf. Ref. 16). In the range where Eq. (7.4) was fitted to the data, it represents all measured properties (thermal and caloric properties) within the experimental uncertainty of the data, except for certain data in a part of the critical region bounded by $0.6\,\rho_c < \rho < 1.4\,\rho_c$ and 645 K $< T <$ 665 K. In this re-

TABLE 5. Parameters and coefficients of the new 38-coefficient equation of state, Eq. (7.4).

i	γ_i	d_i	t_i	a_i
1		1	0	0.233 000 901 3
2		1	2	$-0.140\,209\,112\,8\times10^{1}$
3		2	0	0.117 224 804 1
4		2	1	−0.185 074 949 9
5		2	2	0.177 011 042 2
6		2	3	$0.552\,515\,179\,4\times10^{-1}$
7		3	5	$-0.341\,325\,738\,0\times10^{-3}$
8		5	0	$0.855\,727\,436\,7\times10^{-3}$
9		5	1	$0.371\,690\,068\,5\times10^{-3}$
10		6	3	$-0.130\,887\,123\,3\times10^{-3}$
11		7	2	$0.321\,689\,519\,9\times10^{-4}$
12		8	5	$0.278\,588\,103\,4\times10^{-6}$
13	2	1	5	−0.352 151 113 0
14	2	1	7	$0.788\,191\,453\,6\times10^{-1}$
15	2	1	9	$-0.151\,966\,661\,0\times10^{-1}$
16	2	2	5	−0.106 845 858 6
17	2	3	4	−0.205 504 628 8
18	2	3	6	0.914 619 801 2
19	2	3	13	$0.321\,334\,356\,9\times10^{-3}$
20	2	4	5	$-0.113\,359\,139\,1\times10^{1}$
21	2	5	2	−0.310 752 074 9
22	2	5	3	$0.121\,790\,152\,7\times10^{1}$
23	2	6	2	−0.448 171 083 1
24	2	7	0	$0.549\,421\,877\,2\times10^{-1}$
25	2	7	11	$-0.866\,522\,209\,6\times10^{-4}$
26	2	8	1	$0.384\,408\,408\,8\times10^{-1}$
27	2	8	4	$0.985\,304\,488\,4\times10^{-2}$
28	2	9	0	$-0.176\,759\,847\,2\times10^{-1}$
29	2	11	0	$0.148\,854\,922\,2\times10^{-2}$
30	2	11	3	$-0.307\,071\,906\,9\times10^{-2}$
31	2	11	5	$0.388\,080\,328\,0\times10^{-2}$
32	2	11	6	$-0.262\,750\,521\,5\times10^{-2}$
33	2	11	7	$0.525\,837\,138\,8\times10^{-3}$
34	3	2	13	−0.171 639 690 1
35	3	2	14	$0.718\,882\,362\,4\times10^{-1}$
36	3	3	15	$0.588\,126\,835\,7\times10^{-1}$
37	3	3	24	$-0.145\,593\,888\,0\times10^{-1}$
38	3	5	15	$-0.121\,613\,940\,0\times10^{-1}$

$T_c = 647.14$ K, $\rho_c = 322$ kg/m^3, $R = 0.461\,518\,05$ J/(g K)

gion the 38-coefficient equation is, in contrast to IAPS-84, smooth and continuous and yields physically reasonable results.

8. Discussion of the New Equations of State and Comparison with Experimental Data and Other Equations of State

In the following subsections, the quality of the new equations is discussed based on comparisons with experimental data. Most figures also show comparisons with the Scaling-Law equation[4] in the enlarged critical region and with IAPS-84.[1] In this context, however, the following points should be noted. The official validity range of IAPS-84 does not include temperatures below 273.15 K, pressures above 1000 MPa, and a part of the critical region. When the Scaling-Law equation was originally developed,[4] the parameters of the critical point had not yet been internationally agreed upon.[16] However, to give the reader an impression of values calculated from these two equations, IAPS-84 was also used for comparisons outside its validity range and the Scaling-Law equation was also used in the region very close to the critical point based on the latest values.[16] There were no comparisons with the Hill equation[3] included because of its provisional character.

Since this section only gives a compressed overview of the overall quality of the equations, we will only show a representative sample from the data set that we used for establishing our equations. When discussing both of the new equations, we will only refer to the real part Φ^r [Eq. (7.3) or Eq. (7.4)] which were developed in this work. It is obvious that these real parts must be used according to Eq. (7.1) together with the ideal part Φ^o [Eq. (7.2)] when calculating caloric state values.

With the exception of Fig. 3(a), the figures do not contain any information on the uncertainty of the experimental data because such error bars would have made the figures too crowded. Roughly speaking, the experimental uncertainty corresponds to the scatter of the data, details are given in Ref. 5.

8.1. $pρT$ Data

Figures 3(a) to 3(d) show the relative density deviations of the experimental $pρT$ data from those calculated from Eq. (7.3); the deviations are plotted versus pressure.

We choose for Fig. 3(a) the high resolution of $\Delta\rho/\rho = 3\times10^{-5}$ for the density deviation. In this way we may evaluate the equations of state in the temperature range between 273 and 403 K and at pressures below 100 MPa using a scale which corresponds roughly with the experimental uncertainty. In spite of these extreme requirements in data representation we can see that both equations of state

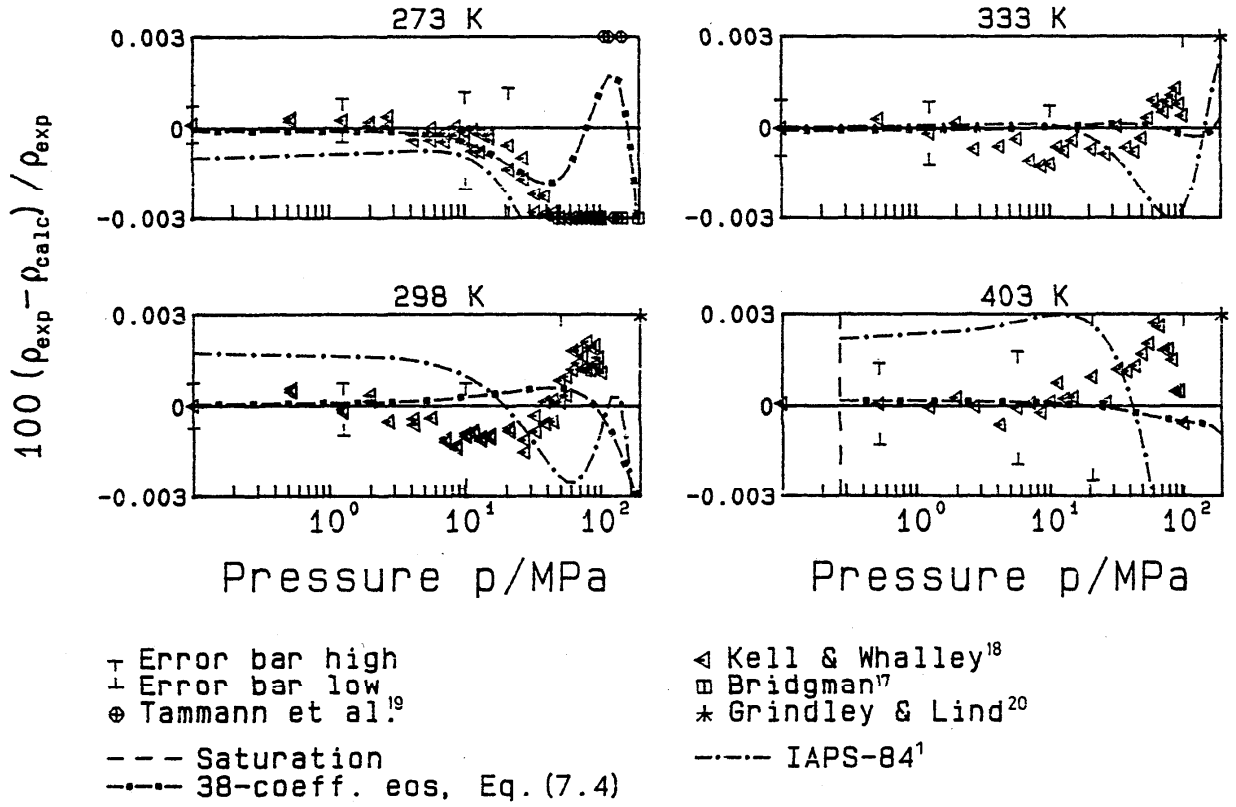

FIG. 3(a). Percentage density deviation of the experimental $pρT$ data from values calculated from the new 58-coefficient equation of state, Eq. (7.3), in a very high resolution with respect to density.

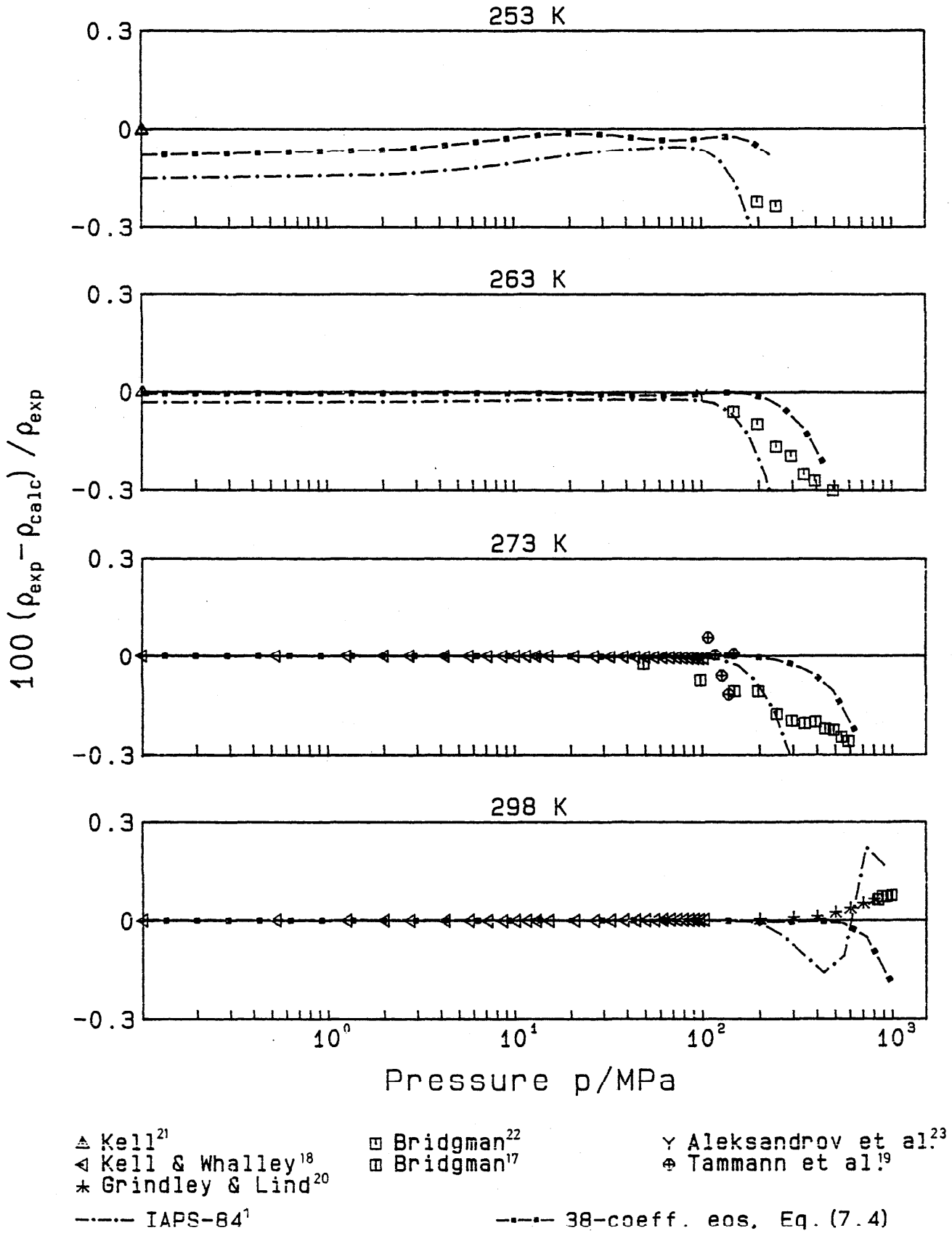

FIG. 3(b). Percentage density deviation of the experimental ppT data from values calculated from the new 58-coefficient equation of state, Eq. (7.3), for the isotherms 253, 263, 273, and 298 K.

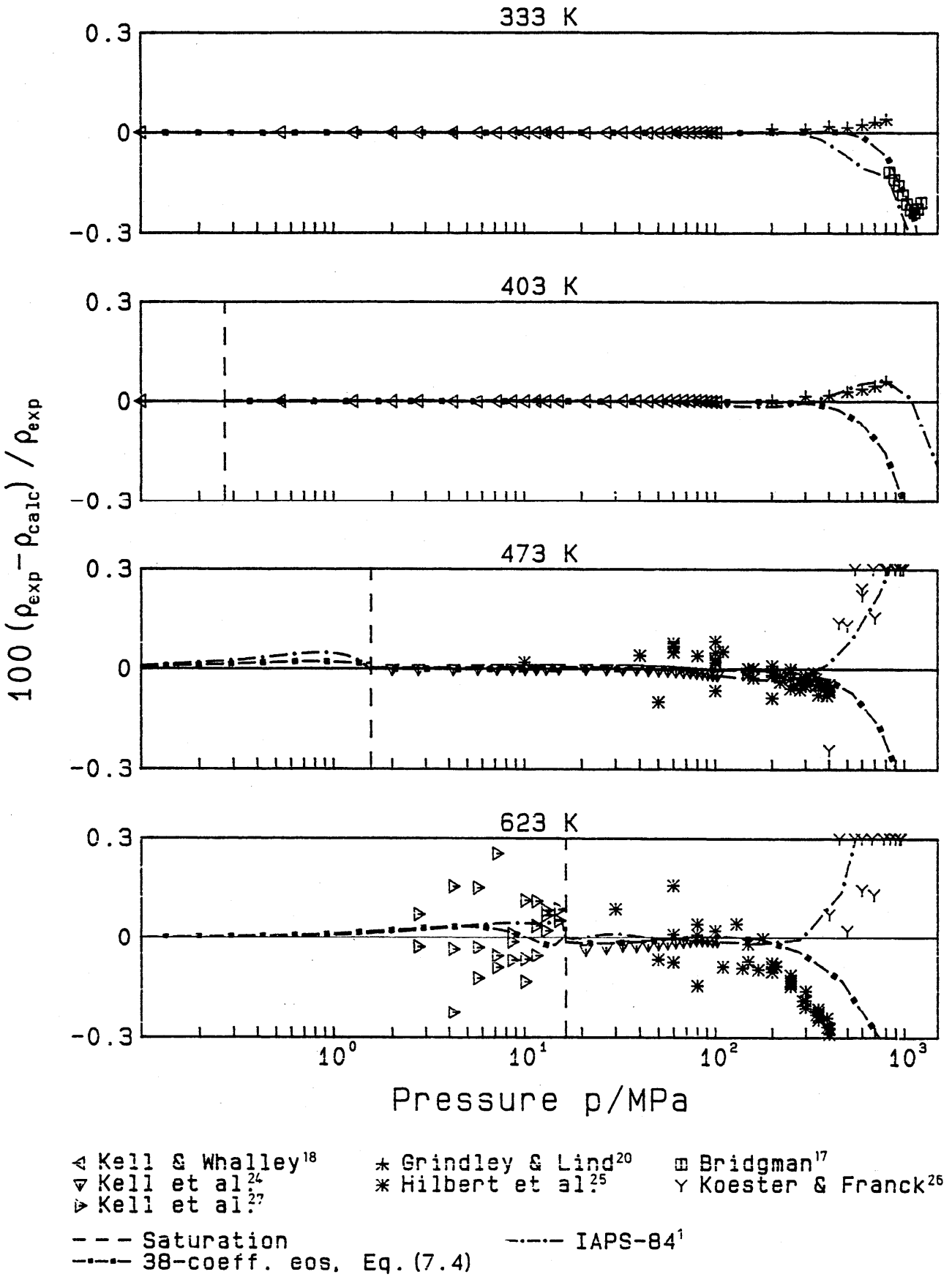

FIG. 3(c). Percentage density deviation of the experimental $pρT$ data from values calculated from the new 58-coefficient equation of state, Eq. (7.3), for the isotherms 333 K, 403 K, 473 K, and 623 K.

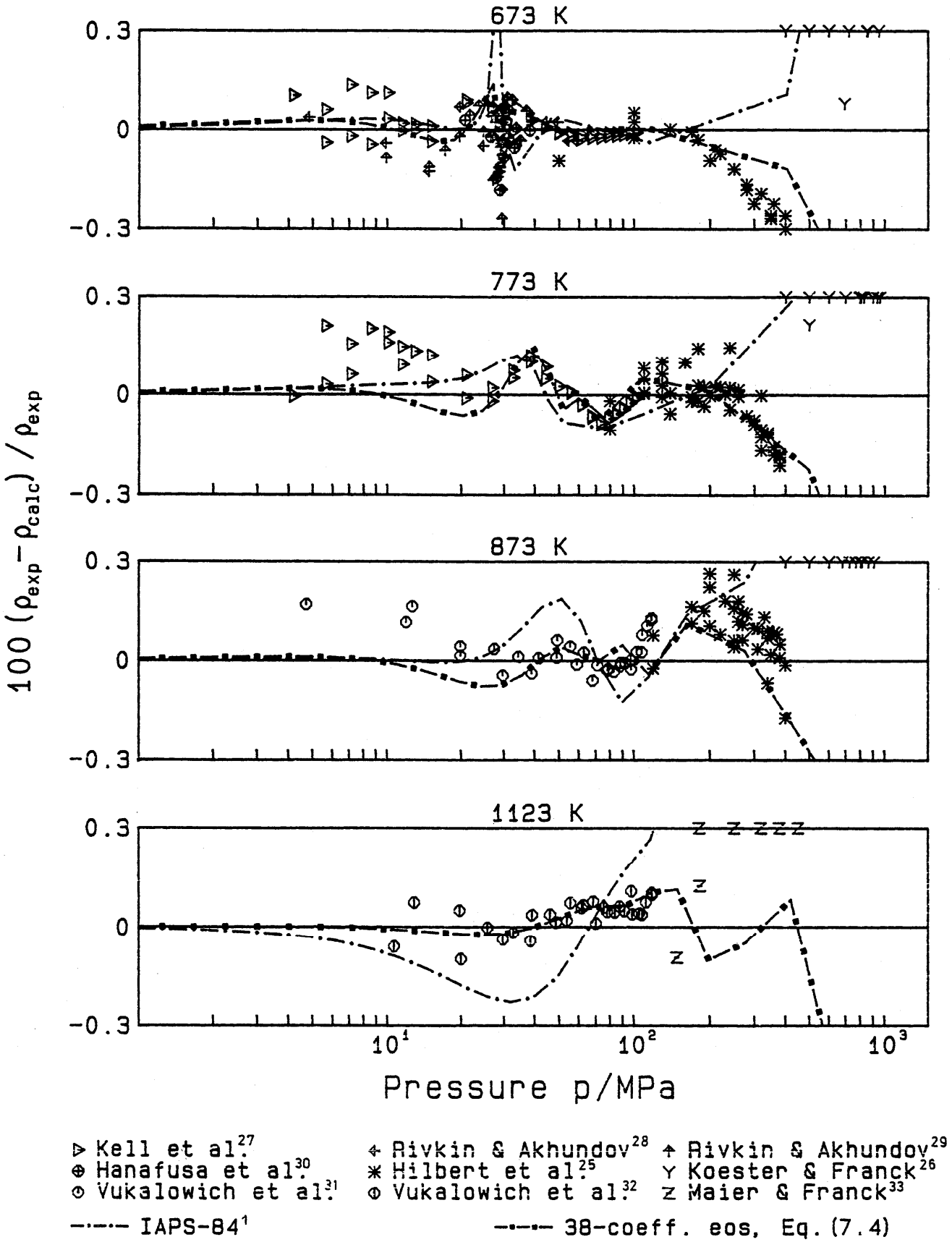

FIG. 3(d). Percentage density deviation of the experimental ppT data from values calculated from the new 58-coefficient equation of state, Eq. (7.3), for the isotherms 673 K, 773 K, 873 K, and 1123 K.

[Eq. (7.3) and Eq. (7.4)] are able to represent the $pρT$ surface within the experimental uncertainty. In contrast to this, IAPS-84 yields for temperatures below 403 K systematically too high or too low values for the density. The systematic deviations of Eq. (7.3) and Eq. (7.4) beyond 30 MPa can be explained by the small inconsistency of the $pρT$ data and the velocity of sound measurements in this region, cf. Kell and Whalley.[18] According to the statements of Kell and Whalley we gave more weight to the speeds of sound in this region. By fitting to the speed of sound data as closely as we did with our equations of state [Eq. (7.3) and Eq (7.4)], we found that the fit to the $pρT$ data became worse; similar results were already observed by Kell and Whalley.[18]

Referring to Figs. 3(b) to 3(d) we can see that the new 58-coefficient equation [Eq. (7.3)] can represent the high-pressure measurements of Grindley and Lind[20] quite well, while IAPS-84 shows oscillating or systematic deviations from the data. The 38-coefficients equation [Eq. (7.4)] represents most of the data in this region better or in the worst case (above 400 MPa) as well as IAPS-84.

From 3(c) and 3(d) we can see that both new equations of state [Eq. (7.3) and Eq. (7.4)] can represent the data of Hilbert *et al.*[25] more closely than does IAPS-84. IAPS-84 deviates considerably more from these measurements in the higher pressure range than do our equations. However, IAPS-84 can represent the data of Maier and Franck[33] as well as of Koester and Frank[26] more closely. Based on our experience it is quite difficult, if not even impossible, to represent all these three data sets within the scatter of the measurements. In favor of the Hilbert *et al.*[25] data, which are consistent with the low-pressure high-quality data of Kell *et al.*,[18,24,27] we chose not to obtain a better representation of the Maier and Franck[33] as well as of the Koester and Frank[26] data, which exhibit an experimental scatter of $\pm$ 1.5%.

Figure 4 shows the relative pressure deviation versus density within the extended critical region, while Fig. 5 is a $pρ$ diagram of the critical region of water substance. Not only the Scaling-Law equation,[4] but also our 58-coefficient equation [Eq. (7.3)] can represent the thermodynamic surface smoothly and continuously within the experimental uncertainty. In contrast to this, IAPS-84 shows obvious systematic deviations from the data in the homogeneous region, and a discontinuity along the saturated liquid line. Our 38-coefficient equation [Eq. (7.4)] also shows systematic deviations along the supercritical isotherms which are greater than the experimental uncertainty, but it yields a smooth and continuous saturated liquid line. Both of our equations of state [Eq. (7.3) and Eq. (7.4)] can represent the phase boundary (dashed line), as defined by the equations internationally recommended by IAPS,[11] much closer than can IAPS-84; cf. also Fig. 14.

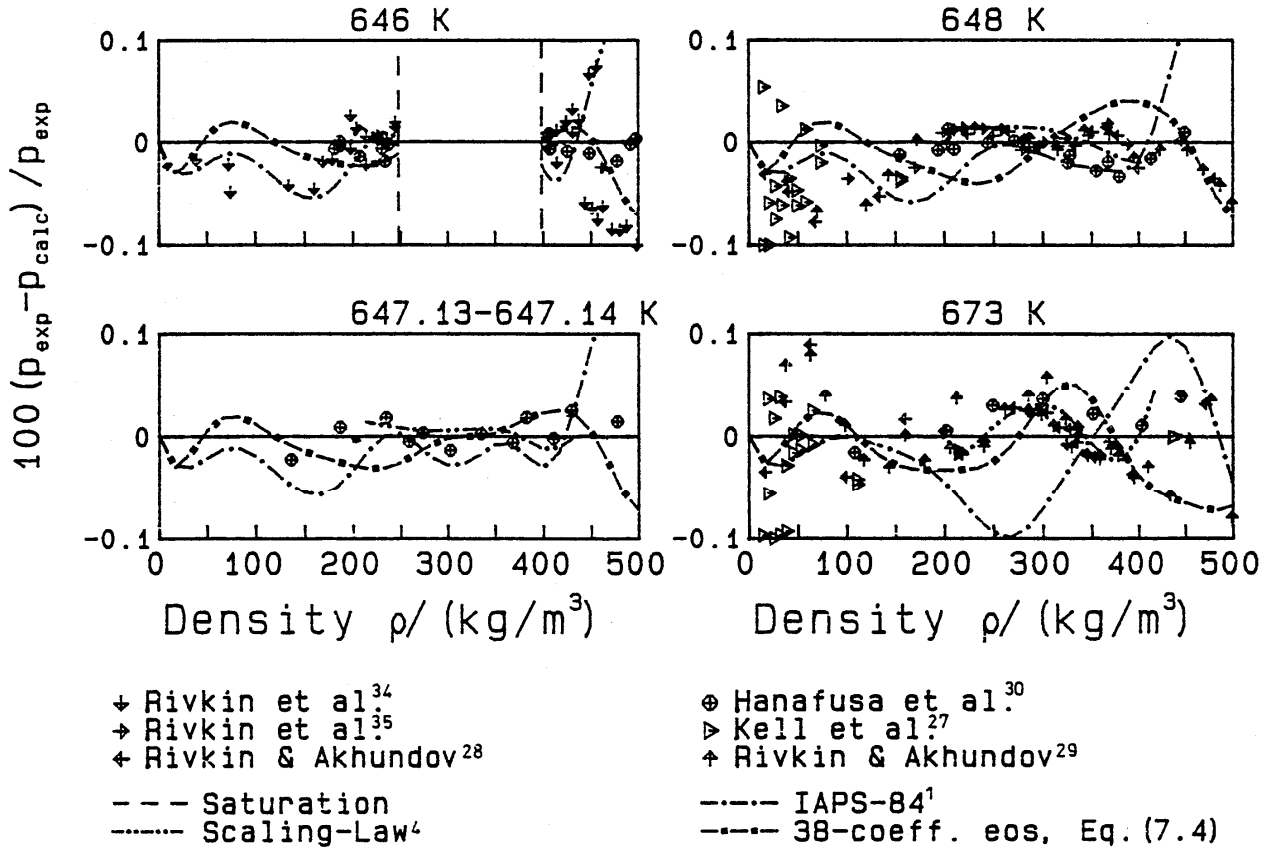

FIG. 4. Percentage pressure deviation of the experimental $pρT$ data from values calculated from the new 58-coefficient equation of state, Eq. (7.3).

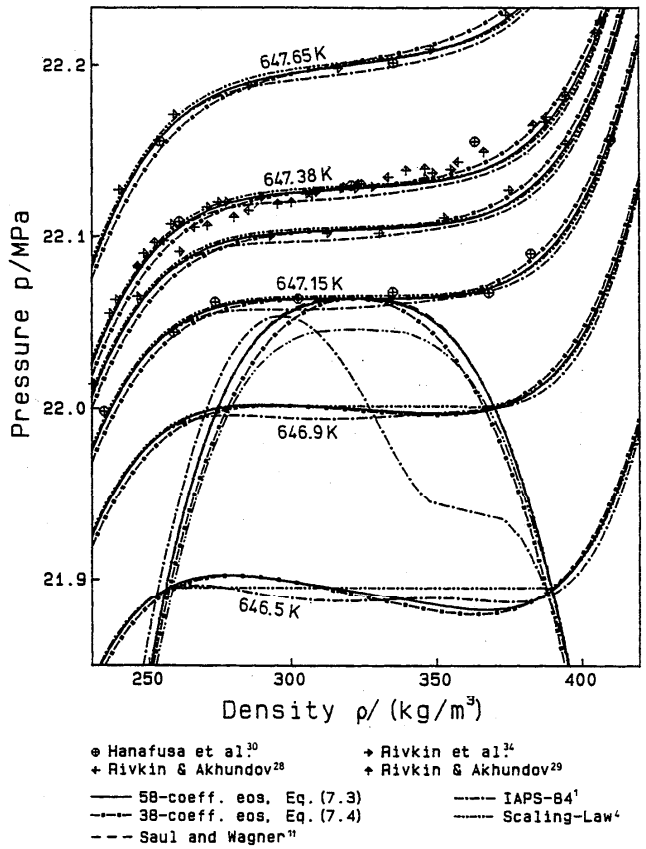

FIG. 5. Representation of the experimental ppT data in the enlarged critical region. In this scale, one can hardly see any difference between the saturation curve calculated from Eq. (7.3) (solid line) and the one calculated using the internationally accepted saturation equations (dashed line, Saul and Wagner[11]). The Scaling-Law equation[4] is based on critical parameters different from those internationally agreed on later[16].

8.2. Isochoric Heat Capacity

Figure 6 shows the relative deviations of the c_v data from our new 58-cofficient equation of state, while Fig. 7 shows the behavior of c_v itself along a near-critical isochore ($\rho = 310\,\mathrm{kg/m^3} = 0.96\,\rho_c$). Those data which are located in both figures to the left of the saturation temperature are measurements of the isochoric heat capacity within the two-phase region. It can be seen in Fig. 6 that our 58-coefficient equation of state can represent all c_v data of both the single phase as well as of the two-phase region within the experimental scatter. The only exception is the near-critical isochore ($\rho = 310\ \mathrm{kg/m^3} = 0.96\,\rho_c$) very close to the saturation temperature in the homogeneous region. The 38-coefficient equation shows a very similar behavior but the region where it undershoots the experimental data starts about 10 K further away from saturation temperature. The same misrepresentation of the data is seen with IAPS-84, but there is an unnatural very steep slope near the saturation line. However, the best representation of the c_v surface of water substance within the critical region is given by the Scaling-Law equation.[4]

8.3. Speed of Sound

Figure 8 shows the relative speed of sound deviations along several isotherms plotted against pressure. The high quality of data representation in the liquid region below 373 K at pressures beyond 100 MPa characterizes our 58-coefficient equation Eq. (7.3). Within this region, IAPS-84 has obvious problems representing the behavior of the surface defined as by the data. When extrapolating IAPS-84 below the triple-point temperature the deviations are as much as 20%. Besides this improvement of data representation in the liquid region, we can also see from Fig. 8 that Eq. (7.3)

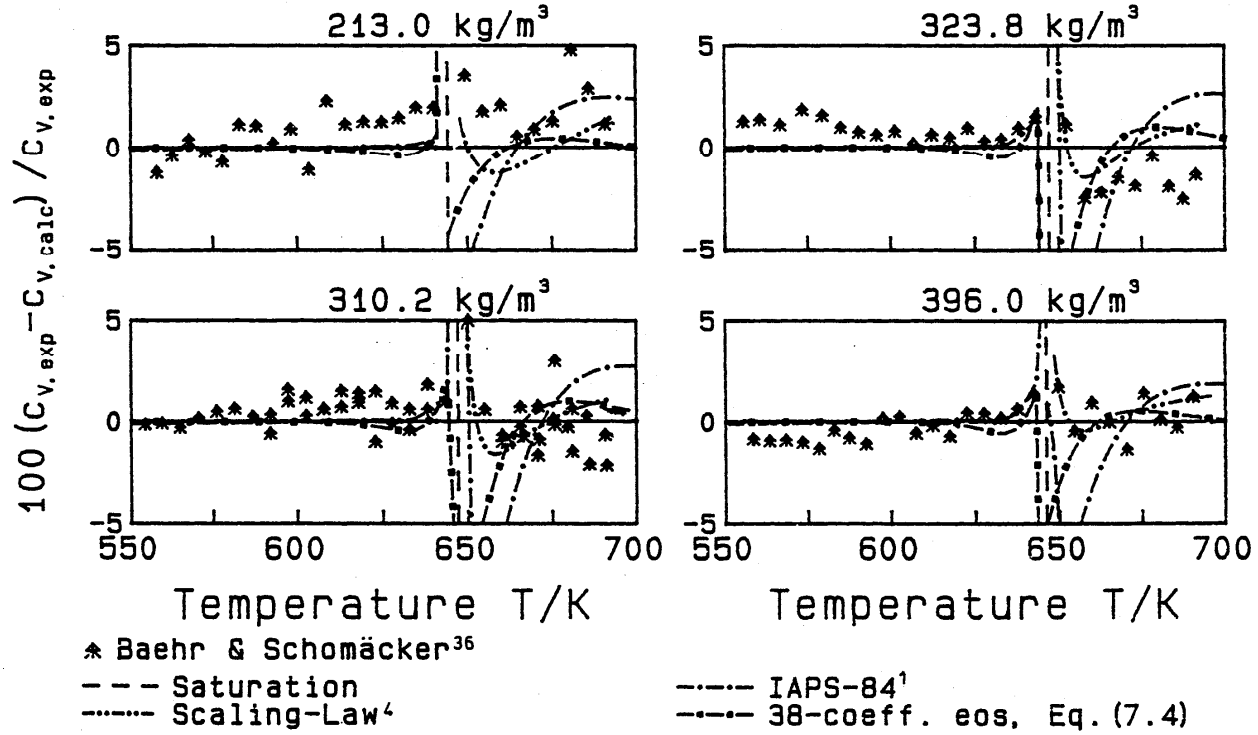

FIG. 6. Percentage deviation of the experimental isochoric heat capacity data from the new 58-coefficient equation of state, Eq. (7.3).

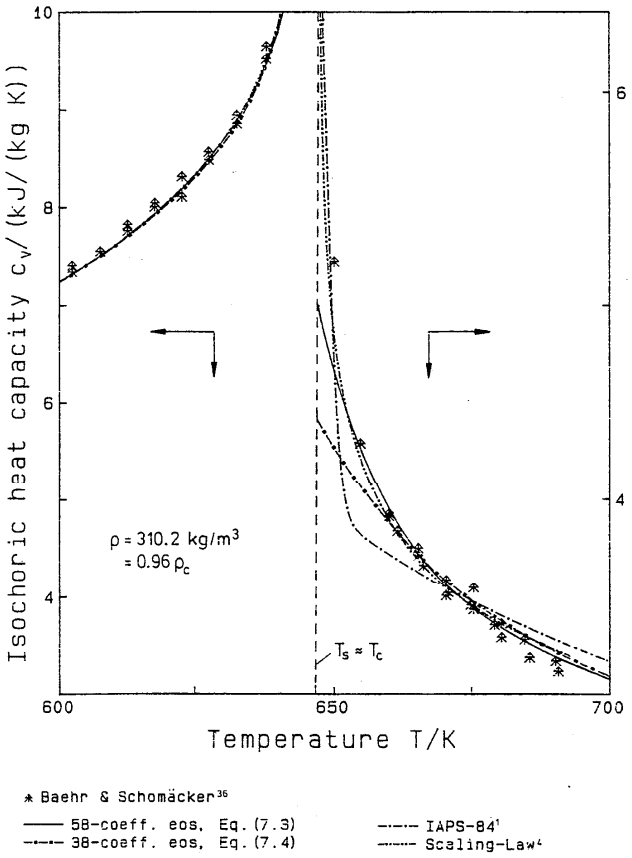

FIG. 7. Representation of the isochoric heat capacity on the near-critical isochore $\rho = 0.96\rho_c$. The c_v scale on the left-hand side corresponds to the data in the two-phase region ($T < T_s$), while the c_v scale on the right-hand side corresponds to data in the homogeneous region ($T > T_s$).

yields a better representation of the speed of sound close to the saturation curve in the vapor state, cf. the 523–532 K isotherm. In the range above 273 K and below 400 MPa (fitted range) our 38-coefficient equation of state is just as able as our 58-coefficient equation to give a high quality of data representation, and it gives a much better fit for pressures beyond 100 MPa than does IAPS-84.

8.4. Isobaric Heat Capacity

Figure 9 gives an impression of the relative deviations of the c_p data from the equations of state. Both of our equations improve the representation of the c_p data in the gaseous region close to saturation along the isobars below 12 MPa (cf. the 5.88 MPa isobar in Fig. 9), where IAPS-84 yields systematically too low c_p values. However, there still remains a discrepancy of about 2% too low c_p values close to saturation. Several attempts were made to correct this systematic deviation. Based on this experience, we concluded that these data are slightly inconsistent with the data of the other properties in this region. In order to avoid a deterioration in the quality of data representation of other properties, we did not fit our equations of state [Eq. (7.3) and Eq. (7.4)] closer to these c_p data.

The supercritical isobars (e.g., the 39.23 MPa isobar) show that, in contrast to the existing equations, for both of our equations of state [Eq. (7.3) and Eq. (7.4)] oscillations at much lower pressures resulting from the "stress" of the critical region have been eliminated.

8.5. Difference of Enthalpy

The relative deviations of the data of Philippi[53] from Eq. (7.3) are given in Fig. 10. The behavior of all equations of state with regard to the measurements looks quite similar. Each of the equations is capable of representing the data within their experimental uncertainty, which is about 2% in most regions. Due to the effect of the temperature uncertainty, the uncertainty in differences of the enthalpy approaches 20% near the critical point.

8.6. Joule–Thomson and Isothermal Throttling Coefficient

Since the tendencies of each of the equations of state to be discussed appear to be very similar with respect to the Joule–Thomson (μ) and the isothermal throttling coefficient (δ_T), these data will be discussed collectively. The comparison with regard to the μ data can be seen in Fig. 11, while Fig. 12 shows the relative deviations of the δ_T data from Eq. (7.3). We can see in both figures that our 58-coefficient equation of state represents the data over the whole temperature and pressure range without systematic deviations within the scatter of the data. Only for temperatures below 550 K do the μ data deviate slightly systematically, but mostly within the scatter, from Eq. (7.3). When considering IAPS-84, we see that it yields systematically too high values with increasing temperature. Our 38-coefficient equation Eq. (7.4) shows the same tendency in a less marked way.

Since the μ and δ_T data are the primary data within this pressure region at temperatures between 431 and 1073 K, they fix the behavior of the second and third virial coefficient (B, C). Hence our 58-coefficient equation is superior to the other equations of state in representing the μ and δ_T data for temperatures above 700 K. Thus, for higher temperatures, we expect more reliable values for B and C from Eq. (7.3) than from the other equations of state.

8.7. Isentropic Temperature–Pressure Coefficient

The comparison of the equations of state with the data of the isentropic temperature–pressure coefficient β_s is shown in Fig. 13. Both of our equations of state [Eq. (7.3) and Eq. (7.4)] represent the data quite well, especially above 293 K.

8.8. Saturation Line

Referring to Fig. 14, the three equations of state behave quite similarly with repsect to the three thermal properties

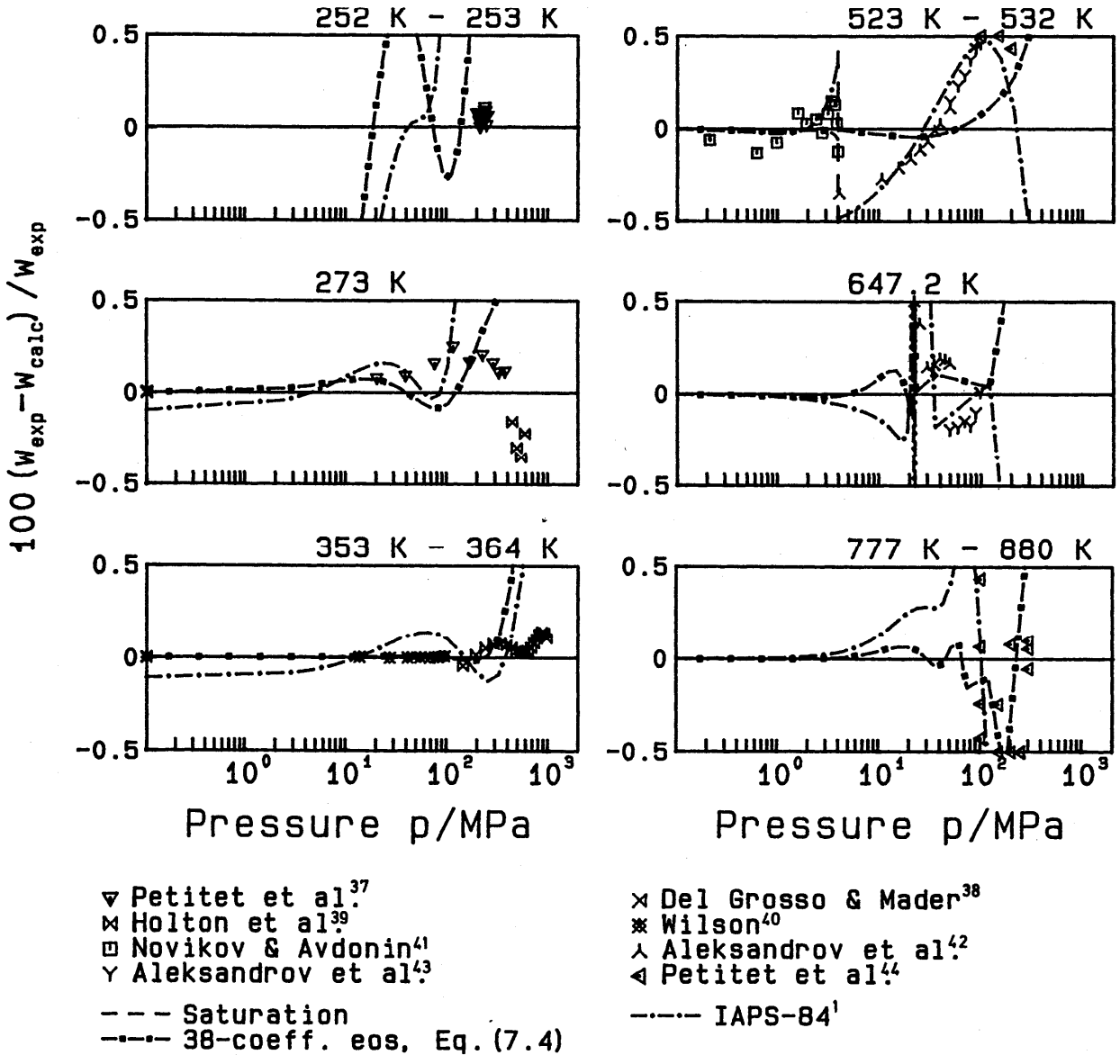

FIG. 8. Percentage deviation of the experimental speed of sound data from the new 58-coefficient equation of state, Eq. (7.3).

vapor pressure p_s, density of the saturated liquid ρ', and density of the saturated vapor ρ''.

The main advantage of our new equations is evident when looking at the deviations of the velocity of sound of the saturated vapor and at deviations of the caloric property $[\alpha]_1^2$, where

$$[\alpha]_1^2 = \left[h' - \frac{T}{\rho'}\frac{dp_s}{dT}\right]_2 - \left[h' - \frac{T}{\rho'}\frac{dp_s}{dT}\right]_1. \qquad (8.1)$$

If one divides $[\alpha]_1^2$ by $(T_2 - T_1)$, then this quotient is nearly identical to the heat capacity of the saturated liquid c_σ for temperatures below 373 K. IAPS-84 shows large systematic deviations from the experimental data, while both of our equations represent all $[\alpha]_1^2$ data within the experimental uncertainty. The excellent agreement of our equations with these data was achieved by a fit to differences of the internal energy along the saturated liquid curve, as indicated in Sec. 5.

When discussing the representation of the speed of sound in the homogeneous region (Sec. 8.3), we already pointed out that both of our equations are capable of representing the speeds of sound in the gaseous region close to saturation significantly better than IAPS-84. This improvement can now be seen, as we would have expected, when looking at the speed of sound of the saturated vapor w'' (cf. bottom diagram in Fig. 14). Both of our equations can represent the w'' data to within about 0.5%, while IAPS-84 yields values for w'' which are about 0.7%–1% too large.

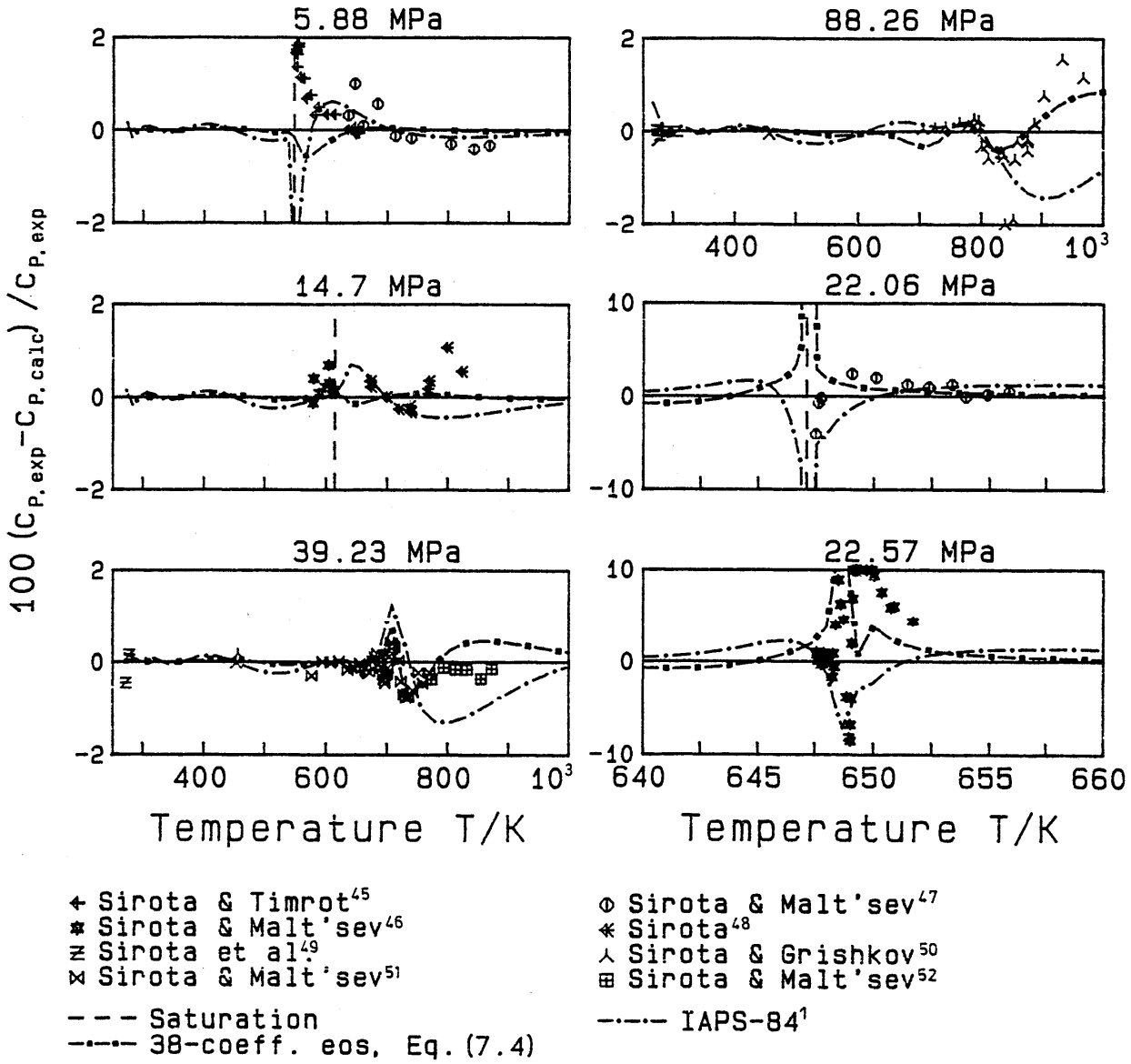

FIG. 9. Percentage deviation of the experimental isobaric heat capacity data from the new 58-coefficient equation of state, Eq. (7.3). The deviation diagrams of the near-critical isobars 22.06 and 22.57 MPa have deviation scales different from the others.

8.9. Virial Coefficients

The behavior of the second and third virial coefficient (B and C) as calculated from several equations is shown in Figs. 15 and 16. Besides the older measurements[62–65] and calculated values[66] of B, these two figures also contain recent experimental results (Eubank *et al.*[68]) and a new correlation (Hill and McMillan[67]) for B and C. For temperatures below 600 K, our 58-coefficient equations shows systematic deviations in comparison to experimental data for B and C. Nevertheless, the entire equation or the equation when truncated after the terms for the third virial coefficient gives a correct representation of all kinds of experimental data in the dilute-gas region.

8.10. Extreme High Pressures

In 1957, Walsh and Rice[70] carried out shock wave measurements in water. Based on the conservation relations for mass, momentum, and energy, they obtained data on the Hugoniot curve (pressure p, enthalpy h, specific volume v data) centered at $p = 0.1$ MPa and $T = 298$ K. Besides these Hugoniot curve data, they also measured $(\Delta h/\Delta v)_p$ by shock reflection measurements at pressures beyond 10 000 MPa. In a succeeding paper, using their own data in the high-pressure regime, Rice and Walsh[71] evaluated several thermodynamic and hydrodynamic properties close to the Hugoniot curve. Their results are based on the assumption that at high pressures $(\Delta h/\Delta v)_p$ is only a function of pres-

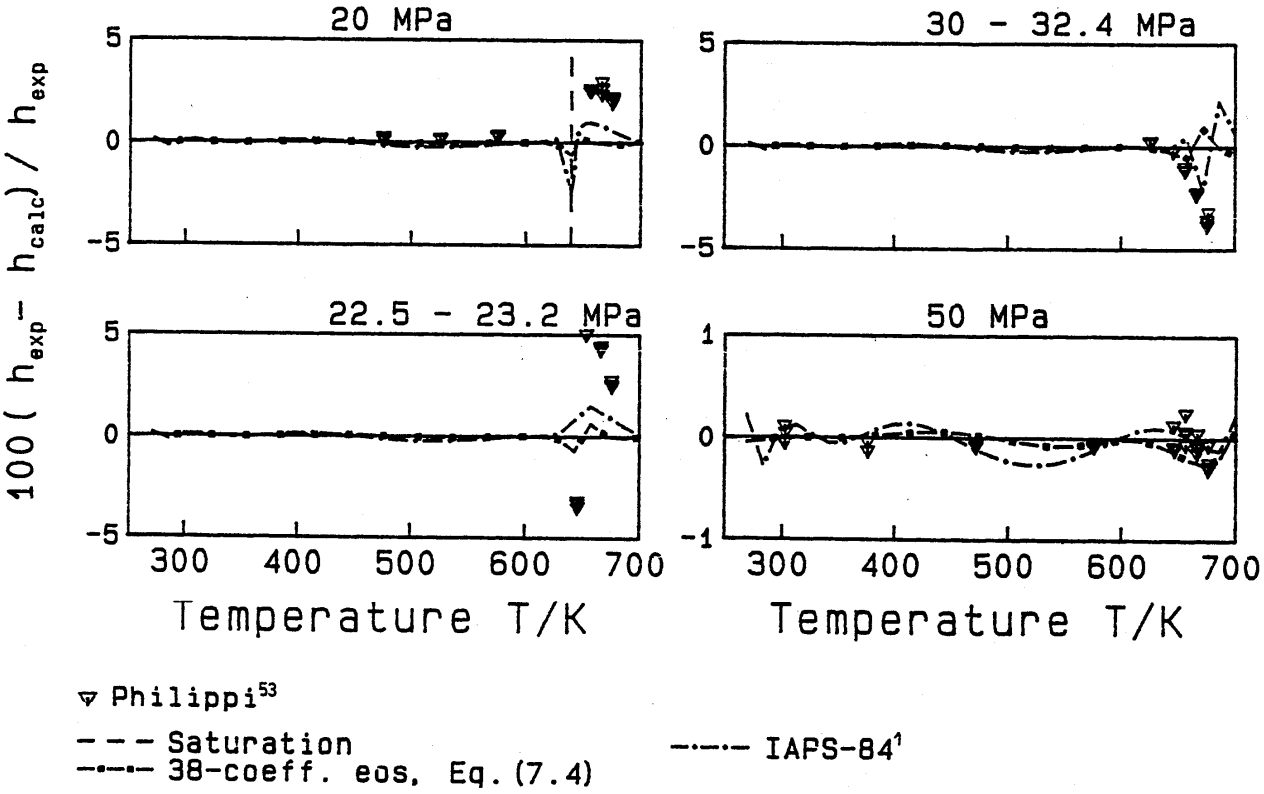

FIG. 10. Percentage deviation of the experimental enthalpy data from the new 58-coefficient equation of state, Eq. (7.3). $\Delta h = h(T_2,p) - h(T_1,p)$ is plotted at the lower temperature T_1 of the temperature interval T_1, T_2. The deviation scale of the 50 MPa isobar is different from the others.

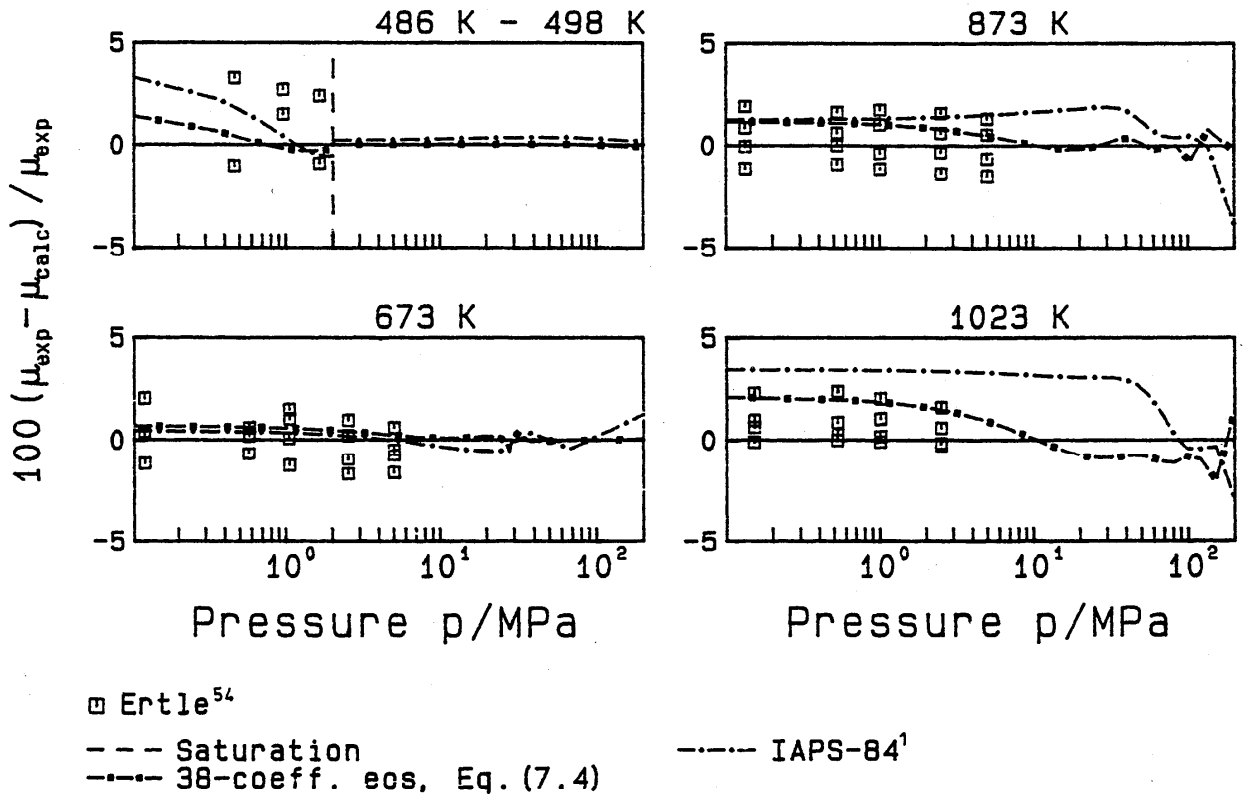

FIG. 11. Percentage deviation of the experimental Joule–Thomson coefficient data from the new 58-coefficient equation of state, Eq. (7.3).

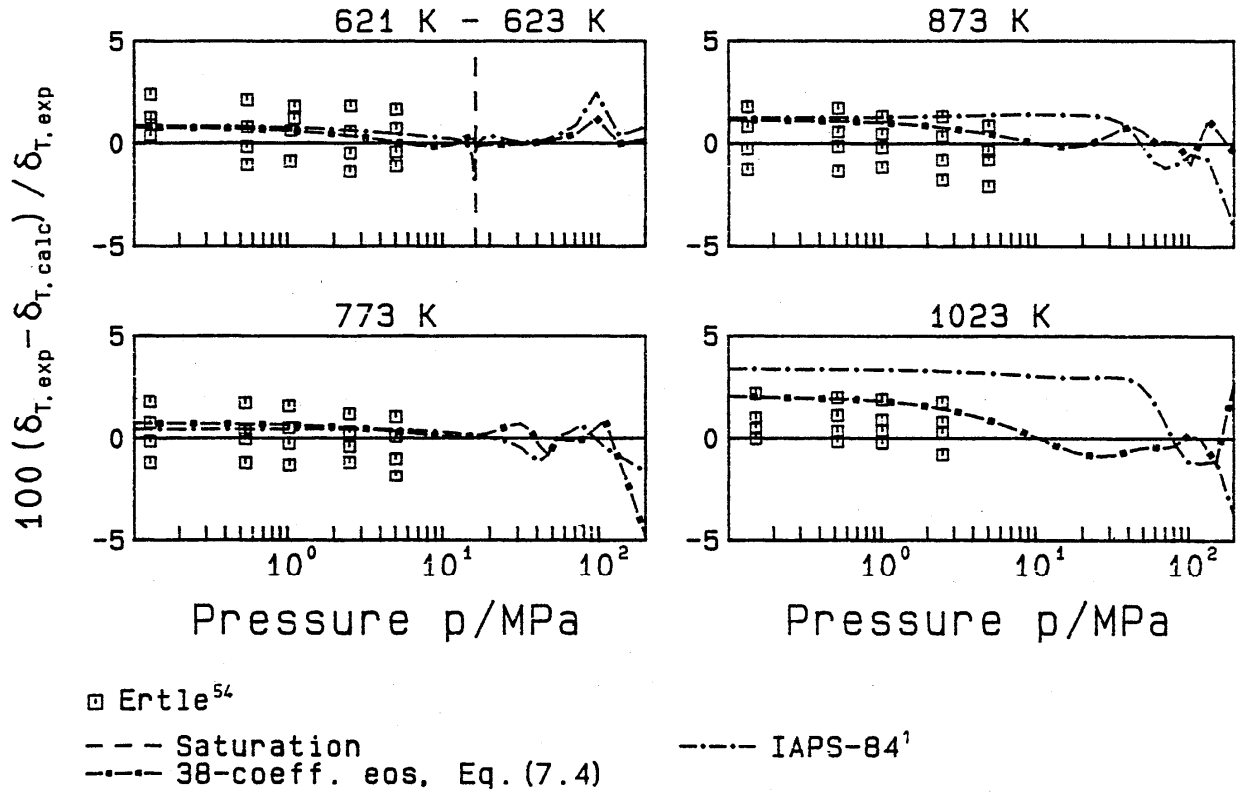

FIG. 12. Percentage deviation of the experimental isothermal enthalpy-pressure coefficient $[\delta_T = (\partial h/\partial p)_T]$ data from the new 58-coefficient equation of state, Eq. (7.3).

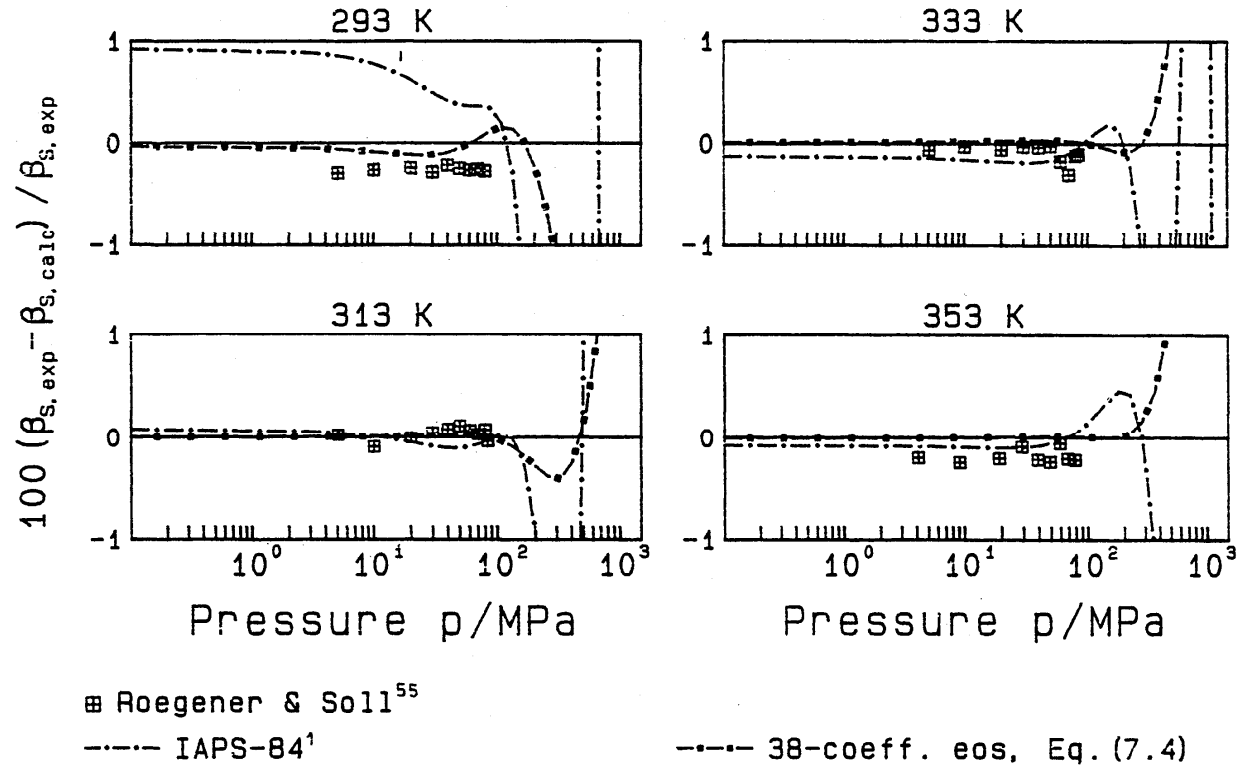

FIG. 13. Percentage deviation of the experimental isentropic temperature–pressure coefficient $[\beta_s = (\partial T/\partial p)_s]$ data from the new 58-coefficient equation of state, Eq. (7.3).

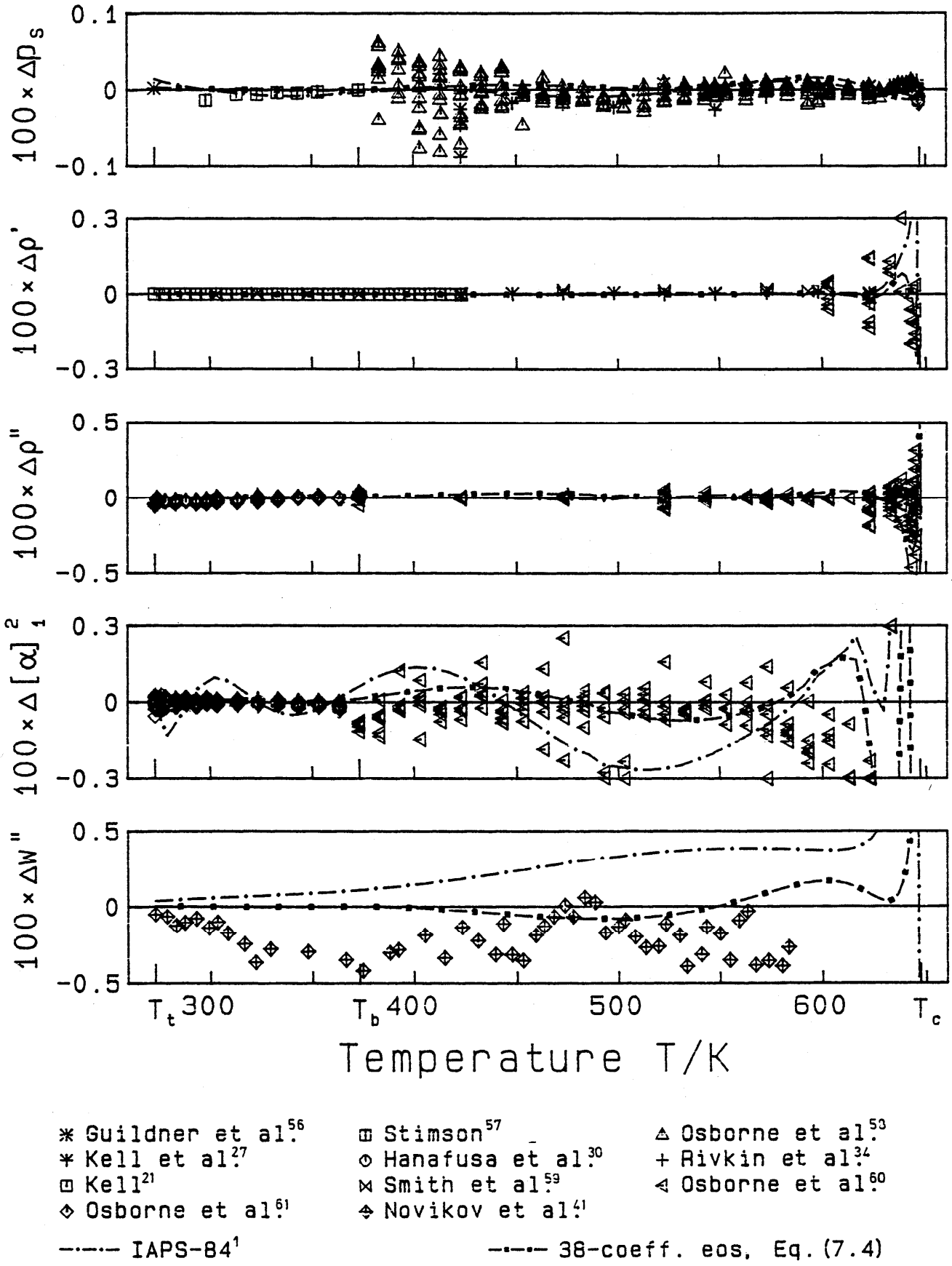

FIG. 14. Percentage deviation $\Delta y = (y_{exp} - y_{calc})/y_{exp}$; $(y = p_s, \rho', \rho'', [\alpha]^2_1, w'')$ of the experimental data on the saturation line from the new 58-coefficient equation of state, Eq. (7.3).

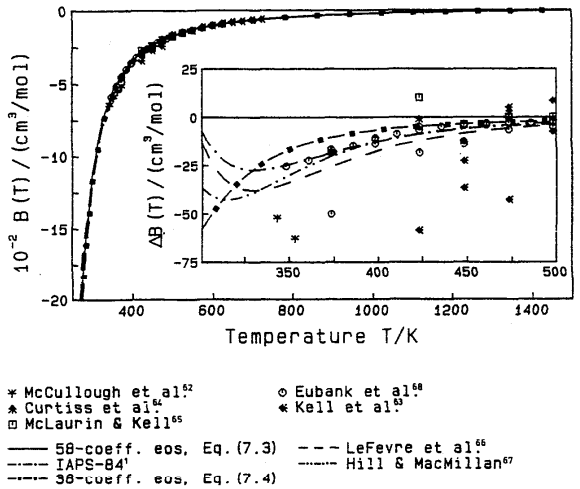

FIG. 15. Experimental second virial coefficients B in comparison with values calculated from several equations.

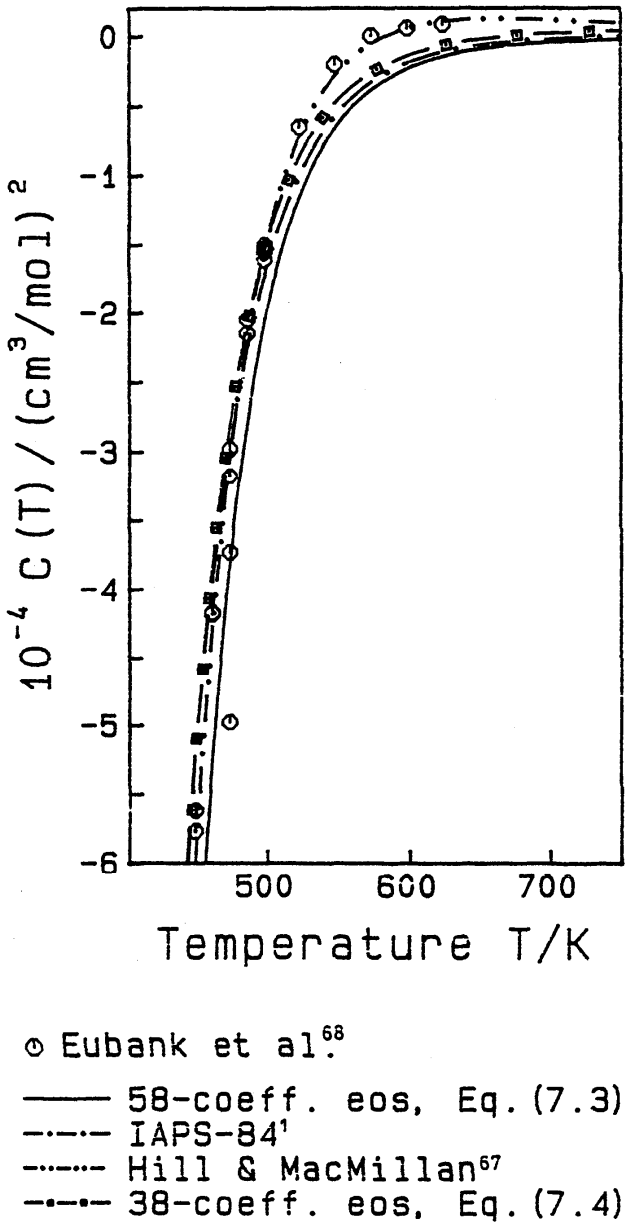

FIG. 16. Experimental third virial coefficients C in comparison with the plot of values calculated from several equations.

sure and that c_p is independent of temperature and has a value of 3.6 kJ/(kg K). To extend their formulation for $(\Delta h/\Delta v)_p$ to lower pressures they had to supplement their own measurements of $(\Delta h/\Delta v)_p \hat{=} (\partial h/\partial v)_p = c_p/(\partial v/\partial T)_p$ with data in the lower pressure range ($p < 10\,000$ MPa). They evaluated $(\partial T/\partial v)_p$ at 2500 MPa from Bridgman's[72] pvT data at that pressure. Taking into account the relatively poor quality of their own $(\Delta h/\Delta v)_p$ data, there is really an excellent agreement with the low-pressure data of Bridgman,[72] although there is an abnormal kink in their $(\partial v/\partial T)_p$ curve. This kink, however, is not the only way one can draw a curve and obtain positive values for $(\partial v/\partial T)_p$. Negative values of the thermal expansion $(\partial v/\partial T)_p$ would be a neccessary condition for the anomaly of intersecting isotherms in the high-pressure range, as predicted by IAPS-84. As a confirmation of the Rice and Walsh[68] data we can see the temperature measurements of Lyzenga and Ahrens[73] along the Hugoniot curve up to 80 000 MPa and the shock wave measurements of Mitchell and Nellis[74] in 1982 up to 83 000 MPa. Based on these temperature measurements, it is obvious that the temperatures calculated by Rice and Walsh deviate systematically beyond 700 K from the data of Lyzenga and Ahrens.[73] At 45 000 MPa we find that the Rice and Walsh temperatures are about 300 K too high. In order to remove this inconsistency, we corrected the temperatures of the pvT data of Rice and Walsh according to the measurements of Lyzenga and Ahrens taking into account the Hugoniot curve measurements of Mitchell and Nellis.[74]

When looking at Fig. 17, which shows the high-pressure surface of water substance, we can see the intersecting isotherms of IAPS-84 as well as those calculated from our 58-coefficient equation of state. The accuracy in representing the pvT data in this high-pressure regime is considered to be sufficient. The comparison of the three equations of state to the "original" Hugoniot data is shown in Fig. 18, and here we see the effect of fitting our 58-coefficient equation of state to the high-pressure pvT data up to 25 000 MPa. Eq. (7.3) is the only equation of state that predicts the true curvature of the Hugoniot curve, while the other equations of state more or less fail to represent the data.

Figure 19 shows a percentage deviation diagram with regard to newer data of the isobaric heat capacity on the 300 K isotherm at pressures up to 1000 MPa. These c_p data, published by Czarnota[69] in 1984, were not taken into account when developing the equation because we overlooked these data at that time. Therefore, this comparison shows how the three equations are able to predict c_p in this difficult region at high pressures up to the melting line. One can see that the 58-coefficient equation, Eq. (7.3), is able to repre-

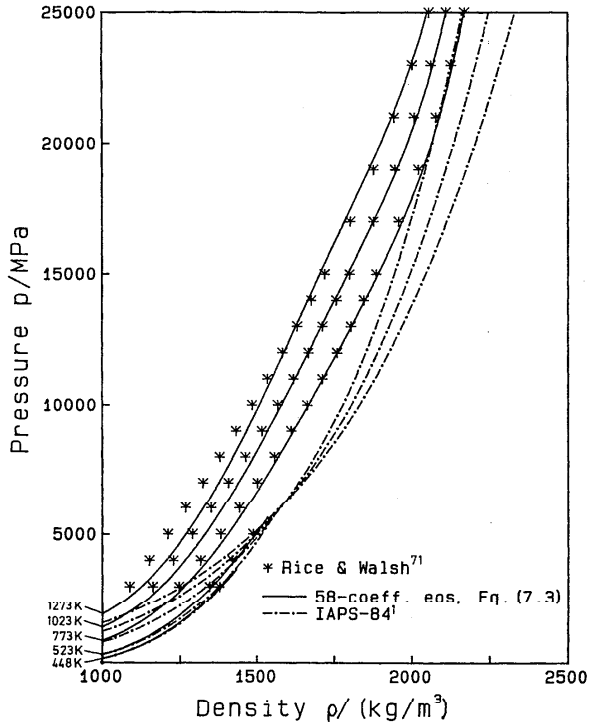

FIG. 17. The $p\rho T$ surface of the new 58-coefficient equation of state, Eq. (7.3), and of IAPS-84 at ultrahigh pressures in comparison with the corresponding data up to 25 000 MPa.

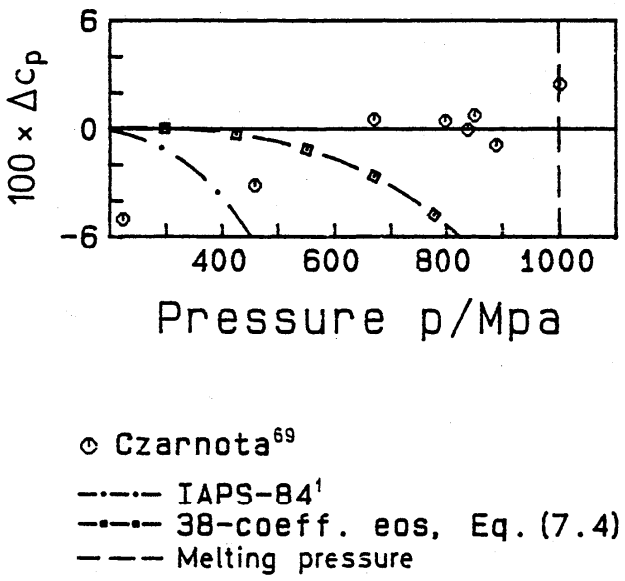

FIG. 19. Percentage deviation $\Delta c_p = (c_{p,\mathrm{exp}} - c_{p,\mathrm{calc}})/c_{p,\mathrm{exp}}$ of experimental high-pressure isobaric heat capacities $c_{p,\mathrm{exp}}$ on the 300 K isotherm from values $c_{p,\mathrm{calc}}$ calculated from the new 58-coefficient equation of state, Eq. (7.3), which was not fitted to these data.

sent these high-pressure c_p data nearly within the experimental uncertainty (approximately $\pm 2\%$). The 38-coefficient equation, Eq. (7.4), also represents the data within its uncertainty for pressures up to 630 MPa, while IAPS-84 yields deviations of about -20% at a pressure of 630 MPa and about -95% at 1000 MPa (melting pressure).

8.11. Metastable States and Spinodals

The group of Skripov (e.g., Skripov[75]) has been involved with the thermodynamic properties of water in the superheated liquid states for several years. They published measurements of $p\rho T$ data (Refs. 76, 77) as well as speed of sound data (Ref. 78). The measurements do not extend far enough into the metastable region to show significant differences in representation by each of the existing equations of state. All the equations of state can represent these data within the estimated experimental uncertainties.

Besides measurements on the superheated liquid, there also exist c_p measurements in the supercooled liquid along the 0.1 MPa isobar of Angell and Sichina.[79] As shown in Fig. 20, our 58-coefficient equation of state can represent these measurements over the entire range of temperature, while IAPS-84 fails below 270 K and our 38-coefficient equation of state below 255 K.

During our investigations of the metastable states, we also tested the method of Kamiri and Lienhard[80] to fix the

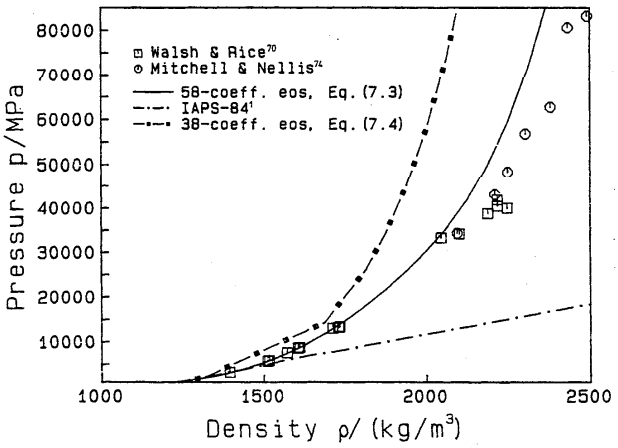

FIG. 18. The original Hugoniot-curve data in comparison with corresponding values calculated from our new equations, Eqs. (7.3) and (7.4), and from IAPS-84. The fitted range of Eq. (7.3) was limited to pressures up to 25 000 MPa.

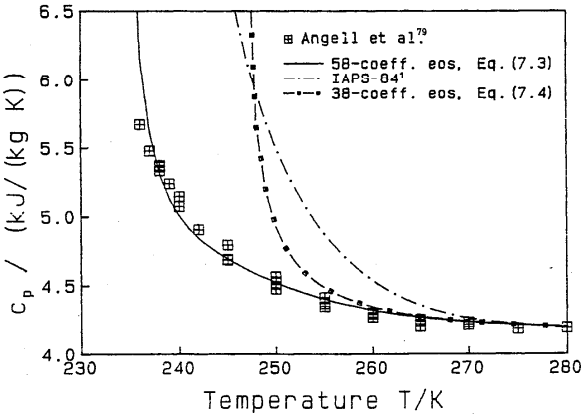

FIG. 20. Representation of c_p in the supercooled liquid along the 0.1 MPa isobar.

surface of an empirical equation of state within the meta- and unstable region. This method shall be described here very briefly. Based on the assumption that a cubic equation of state, here the Himpan equation[81]

$$\frac{p}{RT}=\frac{1}{v-a(T)}+\frac{b(T)}{[v-c(T)][v-d(T)]}, \quad (8.2)$$

can represent the natural behavior of the surface within the two-phase region; this equation is at first fitted to isothermal data of the homogeneous region and to data defining the Maxwell criterion. For each fitted isotherm a set of parameters a, b, c, and d is obtained. Then, the location of the spinodals on a specific isotherm can be found if one uses the condition $(\partial p/\partial \rho)_T = 0$. In addition to this, Kamiri and Lienhard[80] calculated for each isotherm, the slope $(\partial p/\partial \rho)_T$ as well as the pressure p at the critical density ρ_c. In that way one obtains for each isotherm a set of three $p, \rho, (\partial p/\partial \rho)_T, T$ data to which the empirical equation of state may be fitted.

Upon evaluation of this procedure, we found that the parameters a, b, c, and d of the Himpan equation obtained from a nonlinear fit were very sensitive to weighting and to the initial guesses for those parameters. While maintaining the same quality of data representation in the homogeneous region, we could find sets of parameters for a particular isotherm which were not only different by several orders of magnitude but were also of opposite sign. Also, the location of the spinodals differed significantly (pressure and density deviations up to 30%) for these different sets of parameters. In spite of numerous attempts, we were not able to confirm the results of Kamiri and Lienhard. It is our opinion, that the parameters a, b, c, and d of the Himpan equations are not "physical" constants. Therefore, we chose not to constrain the equation of state in the two-phase region according to the method of Kamiri and Lienhard.

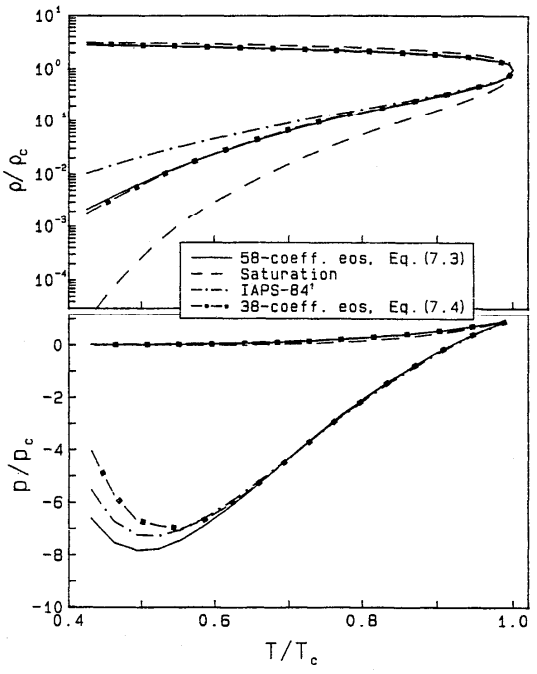

FIG. 21. The spinodals resulting from the different equations of state in a ρT and a pT diagram.

Figure 20 shows that the curvature of the spinodals, resulting from the different equations discussed here, in a ρT as well as in a pT diagram, looks quite similar for all equations. Although the equations have very different functional structures, the behavior does not differ significantly for positive pressures. We would expect that this is in agreement with the natural curvature of the spinodals.

9. Conclusion

Based on the comparisons given in Sec. 8, we have made the following observations. We have found some regions where IAPS-84 has some difficulties. It was shown that our 38-coefficient equation is able to represent the thermodynamic surface of water substance better for pressures below 400 MPa and adequately for higher pressures when compared to IAPS-84. We mainly discussed those properties in selected regions where differences between the different equations of state are visible. Those regions for which our 58-coefficient equation of state Eq. (7.3) can improve the quality of data representation substantially are noted as follows:

1. The range of validity of the new 58-coefficient equation of state [Eq. (7.3)] covers the temperature range between 252 and 1273 K for pressure up to 25 000 MPa or the melting pressure (whichever is lower); this corresponds in pressure to the 25-fold range of validity of IAPS-84.

2. The new equation of state is capable of representing the properties along the saturation line ($p_s, \rho', \rho'', \alpha, w'', c_p$ and w in the gaseous region close to the saturation line) much better than IAPS-84.

3. In the homogeneous region, the new equation of state offers an improvement when compared with IAPS-84 in representing the following properties:

(a) speed of sound for $T < 400$ K and $p > 100$ MPa,
(b) isobaric heat capacity in the gaseous region along isobars below the critical as well as along supercritical isobars near the critical temperature,
(c) isobaric heat capacity in the liquid region for temperatures around 300 K at pressure up to the melting line (about 1000 MPa),
(d) Joule–Thomson and isothermal throttling coefficient for $T > 800$ K.

4. The critical point of the new equation of state corresponds, in contrast to the exisiting equations, to the values recommended by IAPS.[16]

5. The relatively simple structure of the equation aids in programming and speeds up computer execution time.

10. Acknowledgments

The authors are grateful to the Deutsche Forschungsgemeinschaft for financial support of this project. We would also like to thank the members of Working Group A of IAPS for fruitful discussions and helpful hints. The comments of L. Haar, P. G. Hill, J. M. H. Levelt Sengers, and J. T. R. Watson had a significant impact on the final form of this paper.

11. References

[1]J. Kestin and J. V. Sengers, J. Phys. Chem. Ref. Data **15**, 305 (1986).
[2]L. Haar, J. S. Gallagher, and G. S. Kell, Proceedings of the 9th International Conference on the Properties of Steam, edited by J. Straub, and K. Scheffler, (Pergamon, Oxford, 1979), pp. 69–82.
[3]P. G. Hill, A Unified Equation of State for H_2O. Written report to the International Association for the Properties of Steam, 1987.
[4]J. M. H. Levelt Sengers, B. Kamgar-Parsi, F. W. Balfour, and J. V. Sengers, J. Phys. Chem. Ref. Data **12**, 1 (1983).
[5]A. Saul, Fortschr.-Ber. VDI Z. **3**, 149 (1988).
[6]J. R. Cooper, Int. J. Therm. **3**, 35 (1982).
[7]W. Wagner, Fortschr.-Ber. VDI Z. **3**, 39 (1974). Slightly shortened English translation: Report PC/T 15 (IUPAC Thermodynamic Tables Project Centre, Imperial College, London, 1977).
[8]J. Ewers and W. Wagner, VDI-Forsch.-Heft **609**, 27 (1982).
[9]H. Sato, M. Uematsu, K. Watanabe, A. Saul, and W. Wagner, J. Phys. Chem. Ref. Data **15**, 1439 (1988).
[10]U. Setzmann and W. Wagner, Int. J. Thermophysics **10**, 1103 (1989).
[11]A. Saul and W. Wagner, J. Phys. Chem. Ref. Data **16**, 893 (1987).
[12]R. Schmidt and W. Wagner, Report at the Third International Workshop on Equations of State. Thermodynamic Tables Project Centre, Imperial College (London, 1982).
[13]R. Schmidt and W. Wagner, Fluid Phase Equilibria **19**, 175 (1985).
[14]W. Wagner and K. M. de Reuck, International Thermodynamics Tables of the Fluid State-9, Oxygen (Blackwell, Oxford, 1987).
[15]H. W. Woolley, in Ref. 2, pp. 166–175.
[16]J. M. H. Levelt Sengers, J. Straub, K. Watanabe, and P. G. Hill, J. Phys. Chem. Ref. Data **14**, 193 (1985).
[17]P. W. Bridgman, Proc. Am. Acad. Arts Sci. **47**, 441 (1912).
[18]G. S. Kell and E. Whalley, J. Chem. Phys. **62**, 3496 (1975).
[19]G. Tamman and W. Jellinghaus, Z. Anorg. Allgem. Chem. **174**, 225 (1928).
[20]T. Grindley and J. E. Lind, J. Chem. Phys. **54**, 3983 (1971).
[21]G. S. Kell, J. Chem. Eng. Data **20**, 97 (1975).
[22]P. W. Bridgman, J. Chem. Phys. **3**, 597 (1935).
[23]A. A. Aleksandrov, T. S. Khasanshin, and D. K. Larkin, Zhur. Fiz. Khim. **50**, 394 (1976).
[24]G. S. Kell, G. E. McLaurin, and E. Whalley, Proc. Roy. Soc. London A **360**, 389 (1978).
[25]R. Hilbert, K. Tödheide, and E. U. Franck, Ber. Bunsenges. Phys. Chem. **85**, 636 (1981).
[26]H. Köster, and E. U. Franck, Ber. Bunsenges. Physik. Chem. **73**, 716 (1969).
[27]G. S. Kell, G. E. McLaurin, and E. Whalley, Phil. Trans. R. Soc. London **315** A, 235 (1985).
[28]S. L. Rivkin and T. S. Akhundov, Teploenergetika **10**, 66 (1963).
[29]S. L. Rivkin and T. S. Akhundov, Teploenergetika **9**, 57 (1962).
[30]H. Hanafusa, T. Tsuchida, K. Kawai, H. Sato, M. Uematsu, and K. Watanabe, Proceedings of the 10th International Conference of the Properties of Steam, edited by V. V. Sytchev and A. A. Aleksandrov (MIR Moscow, 1986), pp. 180–191.
[31]M. P. Vukalovich, W. N. Zubarev, and A. A. Aleksandrov, Teploenergetika **8**, 79 (1961).
[32]M. P. Vukalovich, W. N. Zubarev, and A. A. Aleksandrov, Teploenergetika, **9**, 49 (1962).
[33]S. Maier and E. U. Franck, Ber. d. Bunsenges. f. Physik. Chem. **70**, 639 (1966).
[34]S. L. Rivkin and G. V. Trojanovskaja, Teploenergetika **11**, 72 (1964).
[35]S. L. Rivkin and T. S. Akhundov, E. A. Kremenevskaja, and N. N. Assadulaeva, Teploenergetika **13**, 59 (1966).
[36]H. D. Baehr and H. Schomäcker, Forsch. Ing.-Wes. **41**, 43 (1975).
[37]J. P. Petitet, R. Tufeu, and B. Le Neindre, Int. J. Therm. **4**, 35 (1983).
[38]V. A. Del Grosso and C. W. Mader, J. Acoust. Soc. Am. **52**, 1442 (1972).
[39]G. Holton, M. P. Hagelberg, S. Kao, and W. H. Johnson, J. Acoust. Soc. Am. **43**, 102 (1968).
[40]W. D. Wilson, J. Acoust. Soc. Am. **31**, 1067 (1959).
[41]I. I. Novikov and V. I. Avdonin, Velocity of Sound in Saturated and Superheated Steam. Report on the 7th Int. Conf. on the Properties of Water and Steam, Tokyo (1968).
[42]A. A. Aleksandrov and D. K. Larkin, Teploenergetika **23**, 75 (1976).
[43]A. A. Aleksandrov and A. I. Kochetov, in Ref. 2, pp. 221–224.
[44]J. P. Petitet, L. Denielou, R. Tufeu, and B. Le Neindre, Int. J. Therm. **7**, 1065 (1986).
[45]A. M. Sirota and D. L. Timrot, Teploenergetika **3**, 16 (1956).
[46]A. M. Sirota and B. K. Mal'tsev, Teploenergetika **9**, 70 (1962).
[47]A. M. Sirota and B. K. Mal'tsev, Teploenergetika **9**, 52 (1962).
[48]A. M. Sirota, Teploenergetika **5**, 10 (1958).
[49]A. M. Sirota, A. J. Grishkov, and A. G. Tomishko, Teploenergetika **17**, 60 (1970).
[50]A. M. Sirota and A. J. Grishkov, Teploenergetika **13**, 61 (1966).
[51]A. M. Sirota and B. K. Mal'tsev, Teploenergetika **6**, 7 (1959).
[52]A. M. Sirota and B. K. Mal'tsev, Teploenergetika **7**, 67 (1960).
[53]R. Philippi. Fortschr.-Ber. VDI-Z. **19**, 13 (1987).
[54]S. Ertle, Dissertation, Technische Universität München, 1979.
[55]H. Rögener and P. Soll, Brennst.-Wärme-Kraft **32**, 472 (1980).
[56]L. A. Guildner, D. P. Johnson, and F. E. Jones, J. Res. Natl. Bur. Stand. **80A**, 505 (1976).
[57]H. F. Stimson, J. Res. Natl. Bur. Stand. **73A**, 493 (1969).
[58]N. S. Osborne, H. F. Stimson, E. F. Fiock, and D. C. Ginnings, J. Res. Natl. Bur. Stand. **10**, 155 (1933).
[59]L. B. Smith and F. G. Keyes, Proc. Am. Acad. Arts and Sci. **69**, 285 (1934).
[60]N. S. Osborne, H. F. Stimson, and D. C. Ginnings, J. Res. Natl. Bur. Stand. **18**, 389 (1937).
[61]N. S. Osborne, H. F. Stimson, and D. C. Ginnings, J. Res. Natl. Bur. Stand. **23**, 197 (1939).
[62]J. P. McCullough, R. E. Pennington, and G. Waddington, J. Am. Chem. Soc. **74**, 4439 (1952).
[63]G. S. Kell, G. E. McLaurin, and E. Whalley, J. Chem. Phys. **48**, 3805 (1968).
[64]C. F. Curtiss and J. O. Hirschfelder, J. Chem. Phys. **8**, 491 (1942).
[65]G. E. McLaurin and G. S. Kell, in Ref. 2, pp. 185–190.
[66]E. J. LeFevre, M. R. Nightingale, and J. W. Rose, Proceedings of the 8th International Conference of Steam, Giens, 1974, p. 480.
[67]P. G. Hill and R. D. Ch. MacMillan, Ind. Eng. Chem. Res. **27**, 874 (1988).
[68]P. T. Eubank, L. L. Joffrion, M. R. Patel, and W. Warowny, J. Chem. Thermodynamics **20**, 1009 (1988).
[69]I. Czarnota, High Temperatures-High Pressures **16**, 295 (1984).
[70]J. M. Walsh and M. H. Rice, J. Chem. Phys. **26**, 815 (1957).
[71]M. H. Rice and J. M. Walsh, J. Chem. Phys. **26**, 824 (1957).
[72]P. W. Bridgman, Proc. Am. Acad. Arts Sci. **74**, 419 (1942).
[73]G. A. Lyzenga, T. J. Ahrens, W. J. Nellis, and A. C. Mitchell, J. Chem. Phys. **76**, 6282 (1982).
[74]A. C. Mitchell and W. J. Nellis, J. Chem. Phys. **70**, 6273 (1982).
[75]V. P. Skripov, Metastable Liquids (Wiley, New York, 1974).
[76]V. N. Chukanov and V. P. Skripov, Teplofizika Vysokikh Temperatur **9**, 739 (1971).
[77]V. N. Evstefeev, V. N. Chukanov, and V. P. Skripov, Teplofizika Vysokikh Temperatur **15**, 659 (1977).
[78]V. N. Evstefeev, V. P. Skripov, and V. N. Chukanov, Teplofizika Vysokikh Temperatur **17**, 252 (1979).
[79]C. A. Angell, M. Oguni, and W. J. Sichina, J. Phys. Chem. **86**, 998 (1982).
[80]A. Kamiri and J. H. Lienhard, A Fundamental Equation Representing Water in the Stable, Metastable and Unstable States (Electric Power Research Institute, Paolo Alto, California, EPRI NP-3328, 1983).
[81]J. Himpan, Monatshefte für Chemie **86**, 259 (1955).

Appendix A1. The Relations of the Helmholtz Function to Other Properties

TABLE A1. Relations of the Helmholtz function Φ to other thermodynamic properties.

Pressure $p = -(\partial f/\partial v)_T$

$$\frac{p(\delta,\tau)}{\rho RT} = 1 + \delta\Phi^r_\delta \tag{A1}$$

Internal energy $u = f - T(\partial f/\partial T)_v$

$$\frac{u(\delta,\tau)}{RT_c} = \Phi^0_\tau + \Phi^r_\tau \tag{A2}$$

Enthalpy $h = f - T(\partial f/\partial T)_v - v(\partial f/\partial v)_T$

$$\frac{h(\delta,\tau)}{RT_c} = \tau^{-1}(1 + \delta\Phi^r_\delta) + \Phi^0_\tau + \Phi^r_\tau \tag{A3}$$

Entropy $s = -(\partial f/\partial T)_v$

$$\frac{s(\delta,\tau)}{R} = \tau(\Phi^0_\tau + \Phi^r_\tau) - (\Phi^0 + \Phi^r) \tag{A4}$$

Gibbs energy $g = f - v(\partial f/\partial v)_T$

$$\frac{g(\delta,\tau)}{RT} = 1 + \delta\Phi^r_\delta + \Phi^0 + \Phi^r \tag{A5}$$

Isochoric heat capacity $c_v = (\partial u/\partial T)_v$

$$\frac{c_v(\delta,\tau)}{R} = -\tau^2(\Phi^0_{\tau\tau} + \Phi^r_{\tau\tau}) \tag{A6}$$

Isobaric heat capacity $c_p = (\partial h/\partial T)_p$

$$\frac{c_p(\delta,\tau)}{R} = -\tau^2(\Phi^0_{\tau\tau} + \Phi^r_{\tau\tau}) + \frac{(1 + \delta\Phi^r_\delta - \delta\tau\Phi^r_{\delta\tau})^2}{1 + 2\delta\Phi^r_\delta + \delta^2\Phi^r_{\delta\delta}} \tag{A7}$$

Velocity of sound $w = \sqrt{(\partial p/\partial\rho)_s}$

$$\frac{w^2(\delta,\tau)}{RT} = 1 + 2\delta\Phi^r_\delta + \delta^2\Phi^r_{\delta\delta} - \frac{(1 + \delta\Phi^r_\delta - \delta\tau\Phi^r_{\delta\tau})^2}{\tau^2(\Phi^0_{\tau\tau} + \Phi^r_{\tau\tau})} \tag{A8}$$

Joule–Thomson coefficient $\mu = (\partial T/\partial p)_h$

$$\mu(\delta,\tau)R\rho = \frac{-(\delta\Phi^r_\delta + \delta^2\Phi^r_{\delta\delta} + \delta\tau\Phi^r_{\delta\tau})}{(1 + \delta\Phi^r_\delta - \delta\tau\Phi^r_{\delta\tau})^2 - \tau^2(\Phi^0_{\tau\tau} + \Phi^r_{\tau\tau})(1 + 2\delta\Phi^r_\delta + \delta^2\Phi^r_{\delta\delta})} \tag{A9}$$

Isothermal throttling coefficient $\delta_T = (\partial h/\partial p)_T$

$$\delta_T(\delta,\tau)\rho = 1 - \frac{1 + \delta\Phi^r_\delta - \delta\tau\Phi^r_{\delta\tau}}{1 + 2\delta\Phi^r_\delta + \delta^2\Phi^r_{\delta\delta}} \tag{A10}$$

Isentropic temperature-pressure coefficient $\beta_s = (\partial T/\partial p)_s$

$$\beta_s(\delta,\tau)R\rho = \frac{1 + \delta\Phi^r_\delta - \delta\tau\Phi^r_{\delta\tau}}{(1 + \delta\Phi^r_\delta - \delta\tau\Phi^r_{\delta\tau})^2 - \tau^2(\Phi^0_{\tau\tau} + \Phi^r_{\tau\tau})(1 + 2\delta\Phi^r_\delta + \delta^2\Phi^r_{\delta\delta})} \tag{A11}$$

Second virial coefficient B

$$B(\tau)\rho_c = \lim_{\delta\to 0}\Phi^r_\delta(\delta,\tau) \tag{A12}$$

Third virial coefficient C

$$C(\tau)\rho_c^2 = \lim_{\delta\to 0}\Phi^r_{\delta\delta}(\delta,\tau) \tag{A13}$$

Appendix A2. Explicit Derivatives of the Helmholtz Function with Respect to the Independent Variables

The derivatives of the Helmholtz function:

$$\Phi = \frac{f}{RT} = \Phi^\circ(\delta,\tau) + \Phi^r(\delta,\tau), \qquad \text{[cf. Eq. (7.1)]}$$

where

$$\Phi^\circ = \ln(\delta) + a^\circ_1 + a^\circ_2\tau + a^\circ_3\ln(\tau) + \sum_{i=4}^{8} a^\circ_i\ln(1 - e^{-\gamma^\circ_i\tau}), \qquad \text{[cf. Eq. (7.2)]}$$

and

$$\Phi^r = \sum_{i=1}^{I_1} (a_i \delta^{d_i} \tau^{t_i}) + \sum_{i=I_1+1}^{I_2} e^{-\delta^{\gamma_i}} (a_i \delta^{d_i} \tau^{t_i}) + (e^{-0.4\delta^6} - e^{-2\delta^6}) \sum_{i=55}^{58} (a_i \delta^{d_i} \tau^{t_i}),$$

[cf. Eq. (7.3)]

with regard to its independent variables δ and τ are necessary for the numerical evaluation of all the equations given in Tables 1, 2, and A1. Since the structure of the Eqs. (7.3) and (7.4) only differs with regard to the (E6-E6) terms, the derivatives of Φ^r are only given for Eq. (7.3). For obtaining the corresponding derivatives for Eq. (7.4) all sums combined with the (E6-E6) terms have to be left out. For I_1 and I_2, respectively, the corresonding values given in Eq. (7.3) and (7.4), respectively, have to be inserted. The derivatives are given as follows:

1st derivative of the dimensionless Helmholtz function with respect to δ:

$$\Phi^\circ_\delta = \delta^{-1}. \tag{A14}$$

$$\Phi^r_\delta = \sum_{i=1}^{I_1} (a_i d_i \delta^{d_i - 1} \tau^{t_i}) + \sum_{i=I_1+1}^{I_2} e^{-\delta^{\gamma_i}} (a_i \delta^{d_i - 1} [d_i - \gamma_i \delta^{\gamma_i}] \tau^{t_i}) + (-2.4e^{-0.4\delta^6} + 12e^{-2\delta^6}) \sum_{i=55}^{58} (a_i \delta^{d_i + 5} \tau^{t_i}) + (e^{-0.4\delta^6} - e^{-2\delta^6}) \sum_{i=55}^{58} (a_i d_i \delta^{d_i - 1} \tau^{t_i}). \tag{A15}$$

1st derivative of the dimensionless Helmholtz function with respect to τ:

$$\Phi^\circ_\tau = a_2^\circ + a_3^\circ \tau^{-1} + \sum_{i=4}^{8} \gamma_i^\circ a_i^0 [(1 - e^{-\gamma_i^\circ \tau})^{-1} - 1],$$

$$\Phi^r_\tau = \sum_{i=1}^{I_1} (a_i \delta^{d_i} t_i \tau^{t_i - 1}) + \sum_{i=I_1+1}^{I_2} e^{-\delta^{\gamma_i}} (a_i \delta^{d_i} t_i \tau^{t_i - 1}) + (e^{-0.4\delta^6} - e^{-2\delta^6}) \sum_{i=55}^{58} a_i \delta^{d_i} t_i \tau^{t_i - 1}. \tag{A16}$$

2nd derivative of the dimensionless Helmholtz function with respect to δ:

$$\Phi^\circ_{\delta\delta} = -\delta^{-2}. \tag{A17}$$

$$\Phi^r_{\delta\delta} = \sum_{i=1}^{I_1} (a_i d_i (d_i - 1) \delta^{d_i - 2} \tau^{t_i}) + \sum_{i=I_1+1}^{I_2} e^{-\delta^{\gamma_i}} (a_i \delta^{d_i - 2} [(d_i - \gamma_i \delta^{\gamma_i})(d_i - 1 - \gamma_i \delta^{\gamma_i}) - \gamma_i^2 \delta^{\gamma_i}] \tau^{t_i}) + (5.76e^{-0.4\delta^6} - 144e^{-2\delta^6}) \sum_{i=55}^{58} (a_i \delta^{d_i + 10} \tau^{t_i}) + (-2.4e^{-0.4\delta^6} + 12e^{-2\delta^6}) \sum_{55}^{58} a_i (2d_i + 5) \delta^{d_i + 4} \tau^{t_i} + (e^{-0.4\delta^6} - e^{-2\delta^6}) \sum_{55}^{58} a_i d_i (d_i - 1) \delta^{d_i - 2} \tau^{t_i}. \tag{A18}$$

2nd derivtive of the dimensionless Helmholtz function with respect to τ:

$$\Phi^\circ_{\tau\tau} = -a_3^\circ \tau^{-2} - \sum_{i=4}^{8} (\gamma_i^\circ)^2 a_i^\circ e^{-\gamma_i^\circ \tau} (1 - e^{-\gamma_i^\circ \tau})^{-2},$$

$$\Phi^r_{\tau\tau} = \sum_{i=1}^{I_1} (a_i \delta^{d_i} t_i (t_i - 1) \tau^{t_i - 2}) + \sum_{i=I_1+1}^{I_2} e^{-\delta^{\gamma_i}} (a_i \delta^{d_i} t_i (t_i - 1) \tau^{t_i - 2}) + (e^{-0.4\delta^6} - e^{-2\delta^6}) \sum_{i=55}^{58} (a_i \delta^{d_i} t_i (t_i - 1) \tau^{t_i - 2}). \tag{A19}$$

1st mixed derivative of the dimensionless Helmholtz function with respect to δ and τ:

$$\Phi^\circ_{\delta\tau} = 0,$$

$$\Phi^r_{\delta\tau} = \sum_{i=1}^{I_1} (a_i d_i \delta^{d_i - 1} t_i \tau^{t_i - 1}) + \sum_{i=I_1+1}^{I_2} e^{-\delta^{\gamma_i}} (a_i \delta^{d_i - 1} t_i [d_i - \gamma_i \delta^{\gamma_i}] \tau^{t_i - 1}) + (-2.4e^{-0.4\delta^6} + 12e^{-2\delta^6}) \sum_{i=55}^{58} a_i \delta^{d_i + 5} t_i \tau^{t_i - 1} + (e^{-0.4\delta^6} - e^{-2\delta^6}) \sum_{i=55}^{58} a_i d_i \delta^{d_i - 1} t_i \tau^{t_i - 1}. \tag{A20}$$

The coefficient of both real parts [Eq. (7.3) and (7.4)] are given with an accuracy of ten significant figures. Nevertheless, it is possible to perform calculations in reduced precision (SINGLE PRECISION or REAL *4). This accuracy is sufficient for the major part of the surface; the differences in using reduced precision as opposed to double precision (DOUBLE PRECISION or REAL*8) are within the accuracy of the experimental data. The only exception is with the critical region. Due to the very flat slope of the isotherms in this region, numeric instabilities will arise when evaluating the Maxwell criterion.

When programming Eq. (7.3) in single or in double precision one has to be aware of rounding errors which can occur when the difference $e^{-0.4\delta^6} - e^{-2\delta^6}$ is evaluated at very low densities. One way to avoid this problem is to expand the power of $e^{-0.4\delta^6} - e^{-2\delta^6} = 1.6\delta^6(1 - 1.2\delta^6)$ for $\delta < 0.2$.